Review

Stereochemistry of Simple Molecules inside Nanotubes and Fullerenes: Unusual Behavior of Usual Systems

Valerij Kuznetsov [1,2]

1   Ufa State Aviation Technical University, K. Marksa, 12, Ufa 450008, Russia; kuzmaggy@mail.ru
2   Ufa State Petroleum Technological University, Kosmonavtov, 1, Ufa 450062, Russia

check for updates

Abstract: Over the past three decades, carbon nanotubes and fullerenes have become remarkable objects for starting the implementation of new models and technologies in different branches of science. To a great extent, this is defined by the unique electronic and spatial properties of nanocavities due to the ramified π-electron systems. This provides an opportunity for the formation of endohedral complexes containing non-covalently bonded atoms or molecules inside fullerenes and nanotubes. The guest species are exposed to the force field of the nanocavity, which can be described as a combination of electronic and steric requirements. Its action significantly changes conformational properties of even relatively simple molecules, including ethane and its analogs, as well as compounds with C–O, C–S, B–B, B–O, B–N, N–N, Al–Al, Si–Si and Ge–Ge bonds. Besides that, the cavity of the host molecule dramatically alters the stereochemical characteristics of cyclic and heterocyclic systems, affects the energy of pyramidal nitrogen inversion in amines, changes the relative stability of cis and trans isomers and, in the case of chiral nanotubes, strongly influences the properties of *R*- and *S*-enantiomers. The present review aims at primary compilation of such unusual stereochemical effects and initial evaluation of the nature of the force field inside nanotubes and fullerenes.

Keywords: nanotube; fullerene; endocomplex; computer simulation; barrier of internal rotation; enantiomer; cis and trans isomers; conformational equilibrium; nitrogen pyramidal inversion

1. Introduction

The history of nanotubes [1,2] and fullerenes [3] spans several decades; the most important stages in understanding of their nature and properties are well represented in recent reviews and books [4–10]. The main directions of practical application of such nanoobjects are connected with creation of new materials [4,7–14], applications in pharmacy and medicine [15–24] and wastewater treatment [25]. These possibilities resulted mainly from the formation of endohedral complexes of fullerenes and nanotubes; the first example, synthesis of lanthanum complexes of C_{60}, was described in [26]. Soon after, by using a suitable solvent, supercritical CO_2, molecular surgery, and plasma ion irradiation methods, a great number of endohedral fullerenes and nanotubes, with metals, nitrogen, hydrogen, boron, noble gases, halogens, sulfur, radioactive isotopes, metal nitrides, water, ammonia, methane, methanol, aromatic hydrocarbons, cyclohexane, heterocycles, metallocenes and biomolecules in their cavities, were obtained [27–64]. The endohedral fullerene complexes inside nanotubes are another type of such species; a recent example is presented in [65]. The structure and properties of hybrid molecule–nanotube and fullerene systems were investigated with both experimental and theoretical methods. In addition to the practical use (such clusters, with unique magnetic and optical properties, are interesting as conductors and semiconductors, effective transporters of drugs in biological systems, and for hydrogen and methane storage) it is important to note that due to the

extensive charge transfer between the carbon cage and the guest molecule, the latter acquires an electric charge [27,29,35–37,43,52,62,66]. Besides that, weak and van der Waals interactions play an important role in the molecular encapsulation [66]. It was shown that flat molecules (benzene, coronene, perylene) tend to align their molecular planes with the nanotube axis. In this case, the chirality of the tubes does not matter, but the tube has an influence on the intermolecular distances for confined species. It was also established that the encapsulation of hydrocarbons in nanotubes is energetically profitable [66]. In the case of armchair (n,n) single-walled carbon nanotubes (SWCNTs) and encapsulated hydrohalogens, the final orientation of the confined molecule depends on the internal diameter of the SWCNT's hollow space and the halogen's nature (F, Cl, Br, I) [67].

Guest species inside nanotubes can move under the action of different forces. This phenomenon is experimentally confirmed for "peapod" systems (fullerenes and endohedral fullerenes in SWCNTs) [27]. Besides that, unique conditions in nanotube cavity make possible numerous chemical reactions. For example, theoretical investigation predicted decreasing of the activation barrier of the Menshutkin S_N2 reaction inside nanotubes [68]. On the other hand, the calculated energy barrier for Cl^- exchange in the S_N2 reaction within nanotubes was higher by 6.6 kcal/mol in comparison with the gas phase [69]. Later, it was shown that SWCNTs may be used as effective nanoreactors for preparative syntheses of inorganic [70] and organic [71–75] products with high yields; it is also possible to achieve enantiomeric excess of the products by using a racemic mixture of *P* and *M* enantiomers of (n,m) chiral nanotubes [76].

All of the foregoing clearly shows that the domestic area of fullerenes and nanotubes can be viewed as the action of a solvent with specific properties. If that is true, then the question arises: how does that affect the conformational preference and other stereochemical properties of the encapsulated molecule?

As indicated by C. Reichardt, "The interactions between species in solvents (and in solutions) are at once too strong to be treated by the laws of the kinetic theory of gases, yet too weak to be treated by the laws of solid-state physics" [77]. This statement is one of the main components of solute–solvent interaction research strategy. Its further development has resulted in two solvent models: implicit (continuum) and explicit (discrete); their comparative effectiveness has been discussed in recent publications [78–84]. In this connection, the endohedral complexes of fullerenes and nanotubes can be viewed as a variety of explicit models. Various approximations based on DFT are usually used as an appropriate computational technique for simulation of the structural, electronic, and conformational properties of such systems. Some of the most useful among them are the PBE, hybrid PBE [85] and wB97XD methods [86]. The author's investigations are connected with the approximation PBE/3ζ (PRIRODA program [87]) that correctly describes the structural, thermochemical, and polar characteristics of endohedral complexes of fullerenes [88–91]. The 3ζ triple-split basis set [92] is a full-electron non-relativistic Gauss-type set containing an accelerating aux-part and polarization functions. This allowed to get a comparative analysis of structural change of different compounds in nanocavity using a single proven method of calculation.

The first example of conformational investigation of simple molecules in the nanocavity was devoted to the examination of the torsion motion of H_2O_2 inside (5,5) and (6,6) armchair SWCNTs, using B3LYP/6-31G(d, p) approximation [93]. Two types of orientation of the O–O bond of the guest molecule inside nanotubes—along and perpendicular to the tube axis—were considered. The H–O–O–H torsion angle τ was varied from 0 to 180° with 10° steps. It was established that, in the case of (5,5) SWCNT, the orientation along the axis corresponds to the more stable endohedral complex compared to the perpendicular one. The main minimum on the potential energy surface (PES) in this case belongs to the conformer with τ = 160°, while for the free H_2O_2 molecule it corresponds to the form with τ = 120°. For the adduct H_2O_2@(6,6), with a larger diameter of the nanotube, both orientations of the guest molecule remain stable; the main minimum for the complex with an O–O bond oriented along nanotube axis corresponds to the conformer with τ = 70°. The effect of the weak O–H···π interaction on the binding of the guest molecule is discussed. Polarization of the nanotube in such complexes was also shown.

In view of the foregoing, the objective of the present work is to discuss the conformational behavior and other stereochemical properties a range of compounds: inorganic species, ethane and its analogs, alcohols, ethers, compounds with double bonds, enantiomers, cyclic and heterocyclic molecules—inside nanotubes and fullerenes in comparison with free state or usual solutions. The main focus is on the influence of the size and chemical composition of nanoobjects as well as of SWCNTs' chirality and diameter of fullerenes on the stability of preference conformation and chemical structure of the guest molecule.

2. Conformational Behavior of Ethane and Its Analogs in Nanotubes

Ethane is the classic object of conformational investigations. After Orville-Thomas' fundamental book [94], there was a noticeable increase in the number of papers, which raised the question: why is the staggered form of ethane more stable compared to the eclipsed one? According to the concepts of theory, the nature of the rotational barrier about a simple bond is generally determined by exchange-repulsion, electrostatic, steric and hyperconjugation effects. Their relative contributions have been widely discussed in the literature [95–110]. On the other hand, spectral data indicate that ethane molecules adsorbed on the surfaces of silver, indium, and potassium exist in the eclipsed conformation [111]. Computer simulation shows that this is not the only example of such an unusual conformational behavior of alkanes. For example, nanoscale confinement (protein binding sites or carbon nanotubes) significantly changes conformations of butane, hexane and tetracosane from trans to gauche-rich helical form [112–114]. It is also known that linear alkanes are adsorbed on the surface of zeolites in a highly coiled conformation [115]. On the other hand, direct observation of conformational changes of a single molecule using transmission electron microscopy (TEM) [116] indicates the presence of only 6% of the CF_2–CF_2 and 20% of CH_2–CH_2 bonds in gauche conformation in a single perfluoroalkyl fullerene molecule inside SWCNT [117]. This qualitatively meets the known conformational data for alkyl chains of free hydrocarbon molecules [94]. However, it should be stressed that citing data refer to the alkane chain that contains fullerenes. Because of this additional factor, the flexibility of the chain links inside the nanotubes may be considerably restricted.

2.1. Ethane

The investigation of adsorption and diffusion properties of ethane within SWCNTs was presented in [118–123]. It has been established that nanotube geometry in some cases plays a definite role in the adsorption activity. The selectivity of adsorption of a binary mixture of ethane and ethylene was also studied. On the other hand, the rotational barriers of methyl-sized groups depend on van der Waals interactions and may vary under the influence of the nanosurface [124]. The first example of conformational transformation of ethane in the nanotube cavity was presented in [125].

Surprisingly, during the calculation (DFT approximation PBE/3ζ), the initial staggered form of ethane inside SWCNT (4,4) spontaneously converted to the eclipsed conformation. Its Hessian, in contrast to the staggered form, did not contain imaginary frequencies (Figure 1).

The relative stability of the staggered form of free C_2H_6 ($\Delta G^{\neq}_{298}$) is 2.5 kcal/mol. It should be noted that this value is slightly underestimated in comparison with data from the literature (2.8–3.04 kcal/mol [94]). In the case of encapsulated ethane, the eclipsed form is more stable than the staggered form at 0.4 kcal/mol. Moreover, both encapsulated forms have a negative electric charge (−0.53), the shortened C–C bond length (r_{C-C} 1.502–1.505 instead of 1.531–1.544 Å for the free molecule) and decreased Mulliken's bond order (O_{C-C} 0.78–0.79 instead of 1.00–1.02). The guest molecule is oriented along the symmetry axis of the nanotube. The distance between hydrogen atoms of ethane and the SWCNT sceleton is 1.7 Å [125].

This relationship was confirmed for other endohedral clusters of ethane with different types of SWCNTs (Table 1, Figure 2) [126–128].
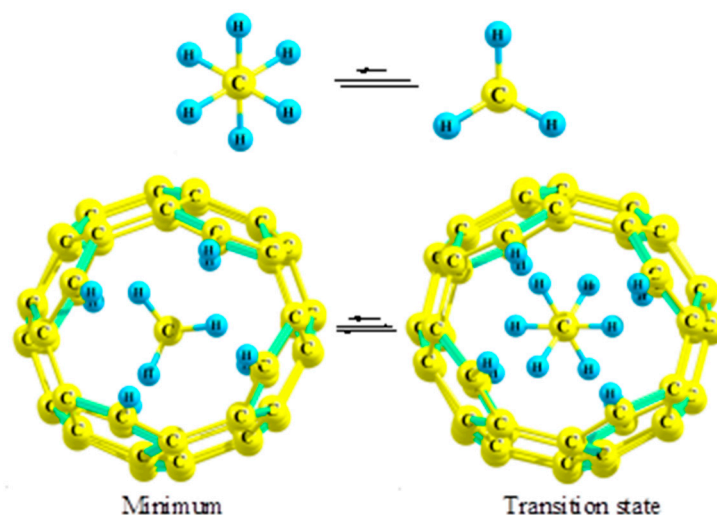
Figure 1. Conformational equilibrium of ethane: free and inside SWCNT (4,4). Adapted with modification [125].

Table 1. Energetical and structural parameters of C_2H_6@nanotubes (PBE/3ζ) [126–128].

Form	$\Delta G^{\ddagger}_{298}$ (kcal/mol)	r_{C-C} (Å)	O_{C-C}	Charge
	C_2H_6			
Staggered	0	1.531	1.02	0
Eclipsed	2.5	1.544	1.00	0
	C_2H_6@(4,4)-closed			
Staggered	0.6	1.495	0.80	−0.54
Eclipsed	0	1.499	0.78	−0.57
	C_2H_6@(6,0)-short			
Staggered	2.0	1.431	0.51	0.72
Eclipsed	0	1.429	0.53	0.73
	C_2H_6@(6,0)-long			
Staggered	1.7	1.434	0.49	0.40
Eclipsed	0	1.432	0.50	0.48
	C_2H_6@(6,0)-CBN			
Staggered	0.9	1.449	0.66	−1.16
Eclipsed	0	1.449	0.66	−1.22

A general characteristic of all clusters is the decrease in C–C bond length with simultaneous reduction of its Mulliken bond order and appearance of positive or negative electric charge on the guest molecule in accordance with the conclusions of [27,29,35–37,43,52,62,66]. SWCNTs with zig-zag geometry, (6,0)-short and (6,0)-long, differ in length (7.11 and 9.34 Å respectively). All endocomplexes demonstrate an evident preference for the eclipsed (or nearly eclipsed) conformation of ethane, although the last cluster with host tube (6,0) with BN fragments (BN nanotubes have been studied in [129–131]) has shown a tendency to reduce the energy differences between both forms, in comparison with carbon-analog: nanotube (6,0)-long [127]. The example of complex C_2H_6@(6,0)-CBN also demonstrates that, with regard to the van der Waals spheres, the inner cavity of the nanotube is densely filled with the guest molecule (Figure 2).
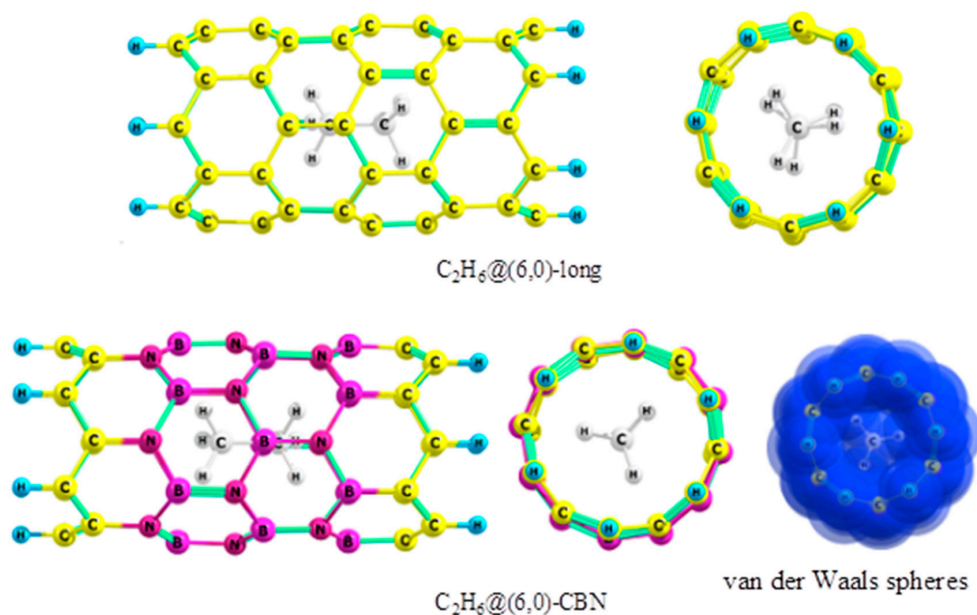
Figure 2. Nanoclusters C_2H_6@SWCNTs. Adapted with modification [126,127].

2.2. Propane

Computer simulation of propane inside two model SWCNTs, (4,4) and (6,0) (PBE/3ζ), shows that staggered conformation in this case is not realized: during the optimization, the guest molecule converts into the fully eclipsed form that cannot exist outside the tube (Figure 3) [132]. This form is more stable than the partially eclipsed conformation (transition state, TS) by 1.6 and 1.2 kcal/mol for the endocomplexes with (4,4) and (6,0) SWCNTs respectively ($\Delta G^{\neq}_{298}$); meanwhile, the calculated barrier of internal rotation for the free propane is 3.0 kcal/mol in favor of the staggered conformer.
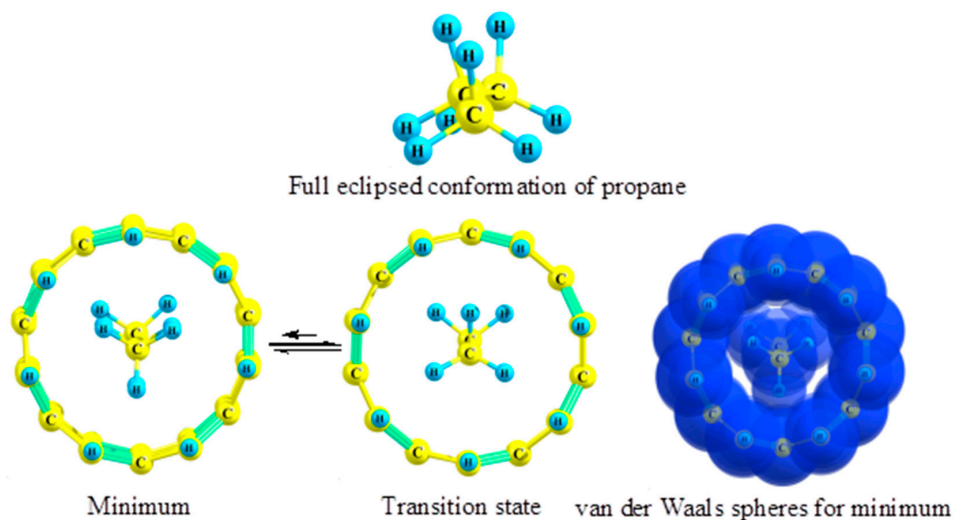

Figure 3. Conformational equilibrium in cluster C_3H_8@(4,4). Adapted with modification [132].

The guest species are characterized by shortened C–C bonds and a small negative electric charge (−0.37−−0.39); the inner cavity of SWCNT is completely filled with the guest molecule [132].

2.3. 2,2,3,3-Tetramethylbutane

According to the electron diffraction data, the structure of gaseous 2,2,3,3-tetramethylbutane (hexamethylethane, C_8H_{18}) corresponds to the staggered form. The central C–C bond length is

1.582 Å [133]; our calculation gives the value 1.590 Å. In this case, the relative stability of the staggered conformer is 8.6 kcal/mol (PBE/3ζ) [134]. However, in endocomplex C_8H_{18}@(5,5), the preferred conformation of the guest molecule is nearly eclipsed (Figure 4).
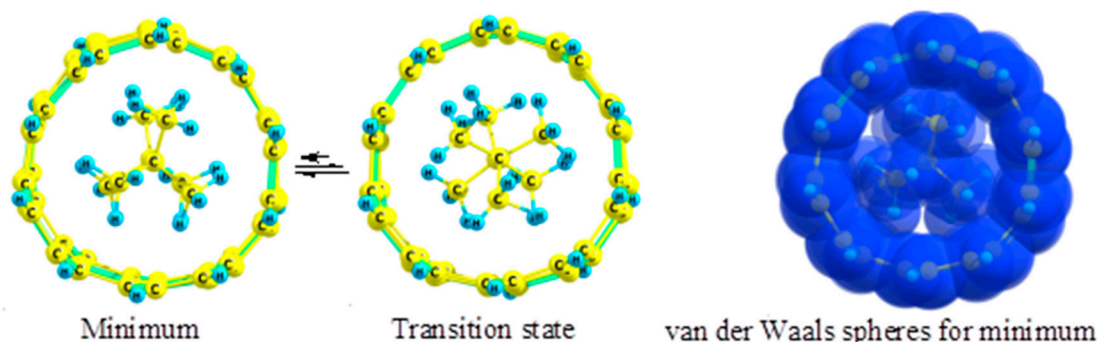

Figure 4. Conformational equilibrium in cluster C_8H_{18}@(5,5). Adapted with modification [134].

The relative stability of the eclipsed form is 0.9 kcal/mol ($\Delta G^{\neq}_{298}$); the length of the central C–C bond is 1.522 Å (shorter by 0.068 Å than in the free alkane). The encapsulated molecule acquires a negative electric charge (−0.93) [134].

2.4. 2,2-Dimethylpropane

2,2-Dimethylpropane (neopentane) is a convenient model system for investigation of the interconnection between the rotational barrier and the molecular environment around the rotator [124,135]. The experimental barrier to internal rotation ($\Delta G_{298}^{\neq}$) is 4.3 kcal/mol [136,137]. However, the conformational behavior of neopentane inside nanotubes differs significantly from that of ethane and its analogs discussed above. Its main feature is a substantial increase in the internal rotation barrier in the case of endocomplexes with SWCNTs of small diameter; TS corresponds to the eclipsed form. According to the PBE/3ζ approximation, the value of $\Delta G_{298}^{\neq}$ for cluster C_5H_{12}@(5,5) with diameter 6.8, Å equals 11.1 kcal/mol, in comparison with 3.8 kcal/mol for the free molecule; the corresponding value for the barrel-shaped SWCNT (7,0) with diameter 9.6 Å is 4.6 kcal/mol. In both cases, the guest molecule has a negative charge (−0.72 and −0.49 for the ground state) [138].

2.5. Fluoroethanes

The conformational behavior of fluoroethanes in the SWCNT cavity is not different from that observed for ethane itself: in the case of a small nanotube diameter, the preferred conformation corresponds to the eclipsed form. Its relative stability varies from 0.8 to 2.3 kcal/mol (Figure 5 and Table 2). An increase in nanotube diameter leads to the preference for a staggered form that, however, remains less stable than for the free molecule [139–143].
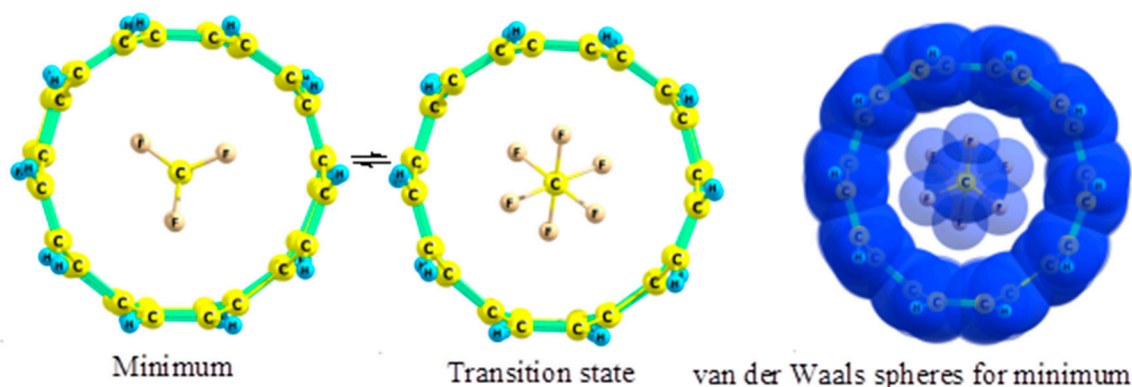

Figure 5. Conformational equilibrium in cluster C_2F_6@(5,5). Adapted with modification [143].

Table 2. Energetical and structural parameters of fluoroethanes (PBE/3ζ).

Form	$\Delta G^{\neq}_{298}$ (kcal/mol)	r_{C-C} (Å)	O_{C-C}	Charge	Reference
		C_2H_5F			
Staggered	0	1.514	1.03	0	[94,139,140]
Eclipsed	3.1 (exp. 3.31)	1.530	1.01	0	
		$C_2H_5F@(4,4)$			
Staggered	0.8	1.487	0.68	−0.19	[140]
Eclipsed	0	1.485	0.73	−0.16	
		$C_2H_5F@(5,5)$			
Staggered	0	1.508	0.96	−0.41	[140]
Eclipsed	2.4	1.522	0.97	−0.40	
		CH_3-CF_3			
Staggered	0	1.507	1.01	0	[139,141,142]
Eclipsed	2.7 (exp. 3.17)	1.521	1.01	0	
		$CH_3-CF_3@(4,4)$			
Staggered	1.2	1.505	0.94	−0.22	[142]
Eclipsed	0	1.518	0.92	−0.20	
		$CH_3-CF_3@(5,5)$			
Staggered	0	1.501	0.99	−0.27	[142]
Eclipsed	2.0	1.513	0.98	−0.26	
		CF_3-CF_3			
Staggered	0	1.565	0.88	0	[139,143]
Eclipsed	4.5 (exp. 4.30)	1.600	0.88	0	
		$CF_3-CF_3@(5,5)$			
Staggered	2.3	1.562	0.88	−0.15	[143]
Eclipsed	0	1.587	0.86	−0.16	
		$CF_3-CF_3@(6,6)$			
Staggered	0	1.539	0.89	−0.13	[143]
Eclipsed	4.2	1.572	0.87	−0.13	

In all cases, the guest molecule has a negative electric charge; besides that, cluster $C_2H_5F@(4,4)$ is characterized by a reduced value of Mulliken C–C bond order (O_{C-C}).

2.6. Ammonia Borane

Ammonia borane (borazane) $H_3B{\leftarrow}NH_3$ has an ethane-like structure; according to microwave measurements, the barrier to internal rotation about the B←N bond equals 2.008–2.047 kcal/mol [144]. The main reasons for the relative stability of staggered form have been discussed in [145]. On the other hand, ammonia borane is a valuable source of hydrogen [146,147]. The creation of effective hydrogen storage is connected with nano-encapsulated $H_3B{\leftarrow}NH_3$ [148,149]. In particular, such systems include ammonia borane clusters with polypyrrol nanotubes [150]. In this connection, the investigation of borazane endocomplexes is an important direction in nanochemistry.

The conformational properties of ammonia borane in the SWCNT cavity are very close to those of ethane. Clusters $H_3B{\leftarrow}NH_3@(4,4)$, $H_3B{\leftarrow}NH_3@(7,0)$ and $H_3B{\leftarrow}NH_3@(8,0)$ demonstrate the preference for the eclipsed form; its relative stability reaches 0.4–0.8 kcal/mol ($\Delta G^{\neq}_{298}$). In some cases, both forms are degenerate in energy [151].

A comparison of free and encapsulated molecules of $H_3B{\leftarrow}NH_3$ (Figure 6) demonstrates that boron atomic charge in the cluster has changed its sign and Mulliken B←N bond order increased almost twofold; all of this indicates the significant redistribution of electron density in the guest molecule.
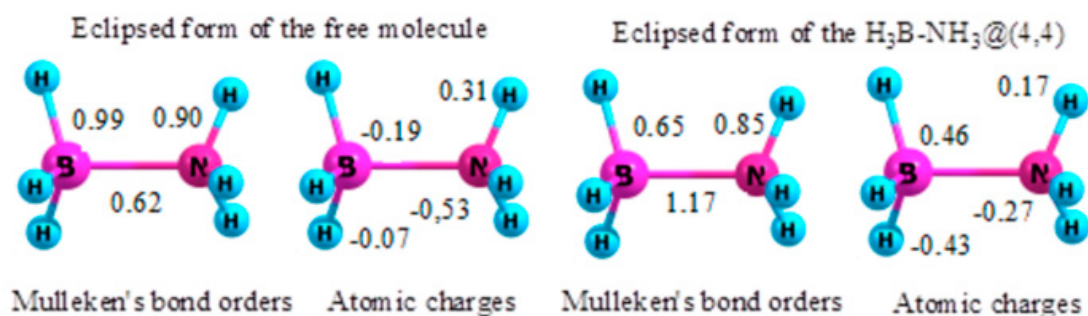
Figure 6. Parameters of free and encapsulated ammonia borane. Adapted with modification [151].

2.7. Disilane and Digermane

Different computational approaches confirmed hindered rotation in disilane, its staggered form being more stable than the eclipsed one [100,152–154]. The calculated rotational barrier (PBE/3ζ, $\Delta G^{\neq}_{298}$, 1.3 kcal/mol [155]) is very close to the one experimentally measured (1.26 kcal/mol [156]). At the same time, computer simulation demonstrates that the height of the barrier in complex Si_2H_6@(8,0) is only 0.4 kcal/mol in favor of the staggered form. In contrast to ethane clusters, the Si–Si bond length of encapsulated disilane is increased by 0.071–0.045 Å in comparison with the free molecule. The growth of the nanotube diameter in the case of cluster Si_2H_6@(6,6) increases the value of $\Delta G^{\neq}_{298}$ to 1.7 kcal/mol (PBE/3ζ, [155]).

The experimental barrier of rotation about the Ge-Ge bond in digermane corresponds to 1.2 kcal/mol [157]. On the other hand, this compound is widely used in epitaxial technology for the creation of mono- or polycrystalline thin films on the surfaces of silicon [158–161], tin [162], and germanium [163,164], with remarkable semiconducting properties. In this connection, endohedral nanocomplexes containing Ge_2H_6 are interesting as an important component in this process.

The conformational behavior of digermane in cluster Ge_2H_6@(8,0) demonstrates a preference for the eclipsed form ($\Delta G^{\neq}_{298}$ 0.8 kcal/mol, in comparison with 1.1 kcal/mol in favor of the staggered form of the free molecule, PBE/3ζ) [165]. As in the previous case, the encapsulated molecule is characterized by a 2% growth in the length of Ge-Ge bond and a strong negative electric charge (−1.37). All other examined clusters—Ge_2H_6@(5,5), Ge_2H_6@(6,6) and Ge_2H_6@(7,7)—with a greater nanotube diameter exhibit a preference for the staggered conformation ($\Delta G^{\neq}_{298}$ 1.1–1.5 kcal/mol) and electric charge (−0.12−−0.97) on the guest molecule [165].

Thus, the action of the force field inside the nanocavity, understood as a combination of electronic and steric requirements, shifts the conformational equilibria of ethane and its analogs inside nanotubes of relatively small diameter (with the exception of neopentane) to the eclipsed form. This is accompanied by a significant change in the central bond length and the bond order.

3. Conformational Behavior of Other Acyclic Molecules in Nanotubes

3.1. Hydroxyborane

In terms of structural chemistry, acyclic derivatives of boron and boronic acids are interesting because of the partially double nature of the B–O bond; as a result, their preferred conformation corresponds to the planar form [166,167]. The rotation barrier lies within 8.5–13.8 kcal/mol [168–170]. According to the PBE/3ζ approximation, the orthogonal conformation—TS for the molecule of hydroxyborane, H_2B–OH—is less stable than the planar form ($\Delta G^{\neq}_{298}$) by 13.9 kcal/mol (Figure 7) [171].

However, in the case of cluster H_2B-OH@(6,0), the value of $\Delta G^{\neq}_{298}$ becomes only 3.8 kcal/mol (3.66 times lower); the increase in the SWCNT diameter, as in the case of H_2B-OH@(6,6), leads to a higher barrier of rotation close to the free molecule (13.4 kcal/mol). The guest molecule in both cases is characterized by electric charge and—for cluster H_2B-OH@(6,0)—by a 1.4% decrease in the length of the B–O bond [171].
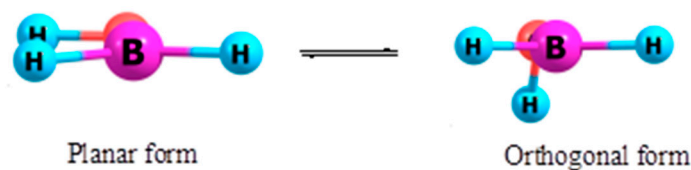
Planar form   Orthogonal form

Figure 7. Conformational equilibrium of hydroxyborane. Adapted with modification [171].

3.2. Diborane (4)

A hypothetical diborane (4) is the boron analog of ethylene. Due to the nature of the boron–boron bond, it represents a model system with non-classical multi-centered bonds [172,173]. The PES of this compound contains three stationary points that correspond to the structures **A** (C2v symmetry), **B** (D2d), and **C** (D2h) [174] (Figure 8).
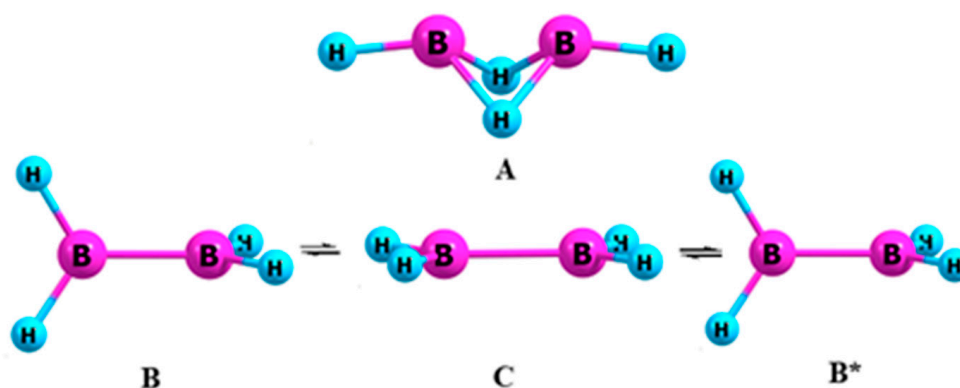

Figure 8. Forms (**A**–**C**) of diborane. Adapted with modification [175].

The first matches the global minimum; the orthogonal conformer **B** is less stable than **A** by 2.9 kcal/mol [CCSD(T)/6-311++G (d,p)] [174] or by 3.0 kcal/mol (PBE/3ζ [175]). It turns into its inverted form (**B***) via the TS—a planar structure **C** with a barrier of 17.9 kcal/mol [175].

All examined SWCNT clusters demonstrate a significant shortening of the B–B bond length in all forms and a relatively high negative electric charge on the guest molecule. Besides that, form **A** belongs to the main minimum on the PES, but differences in energy between **A** and **B** increase 2–4.5 times. The height of the rotation barrier about the B-B bond in endocomplexes is lowered compared with a free molecule; for clusters B_2H_4@(4,4) and B_2H_4@(7,0), it lies in the interval 3.1–5.7 kcal/mol. The growth of the nanotube diameter in complexes B_2H_4@(5,5) and B_2H_4@(8,0) leads to an increase in this value (14.1–17.4 kcal/mol relative to the form **B**) [175].

3.3. Dialane (4)

Dialane (4), Al_2H_4, in contrast to diborane, really exists in two forms: salt-like structure **A** and orthogonal **B** [176,177]. The first corresponds to the global minimum on the PES. The last may be converted into invertomer **B*** via TS—planar conformation **C** (Figure 9) [178].

According to the results of computer simulation, the conformational equilibrium between **B** and **C** forms in clusters Al_2H_4@(5,5), Al_2H_4@(8,0) and Al_2H_4@(9,0), contrary to the free molecule, is completely shifted to the planar form **C**: the appropriate $\Delta G_{298}^{\neq}$ values lie in the interval 2.3–4.5 kcal/mol; $\Delta E_0^{\neq}$ corresponds to 1.4–4.2 kcal/mol (Figure 10). In all cases, the guest molecule has a strong negative electric charge [178].

The authors [107] suggested a decisive role of all seven molecular orbitals in the origin of the rotational barrier in ethane. But the common number of MO's in nanoclusters is very high. That is why we analyzed only HOMO and LUMO orbitals of dialane (4), as well as SWCNT (8,0) and cluster Al_2H_4@(8,0), using PBE/3ζ and PBE/cc-pVDZ approximations [178] (Figure 11).

The main difference between the free molecule and cluster is connected with a notable increase in the HOMO energy in the last case; this is also true for the nanotube itself. Thank to this, the energy gap ΔE for complex Al_2H_4@(8,0) is decreased by 28–34 times compared to free dialane. According to the molecular diagrams, HOMO is localized on the carbon atoms of nanotubes; the highest-energy MO connected with the guest molecule (the planar form of dialane) corresponds to the HOMO-3 level with the energy of −5.3350 eV (PBE/3ζ). Similar results were obtained using PBE/cc-pVDZ approximation.

All this points to the significant transformation of the orbital structure of the endocomplex, which may be a possible reason for the change in conformational behavior of the guest molecule.
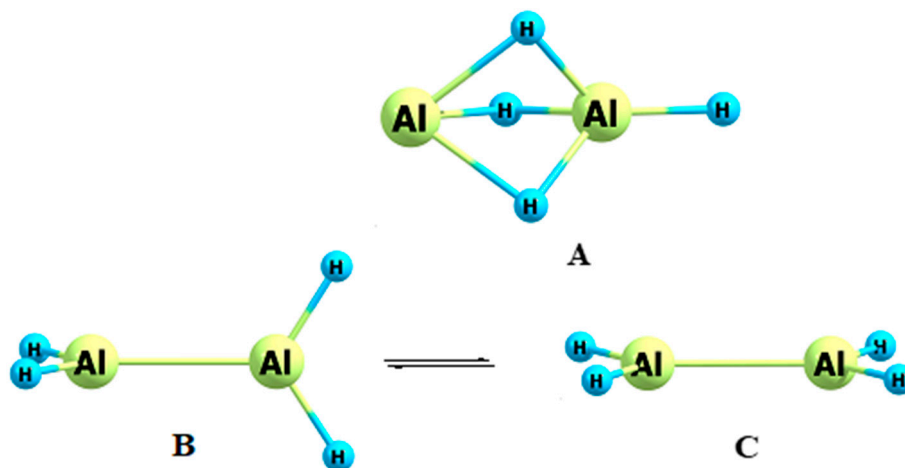

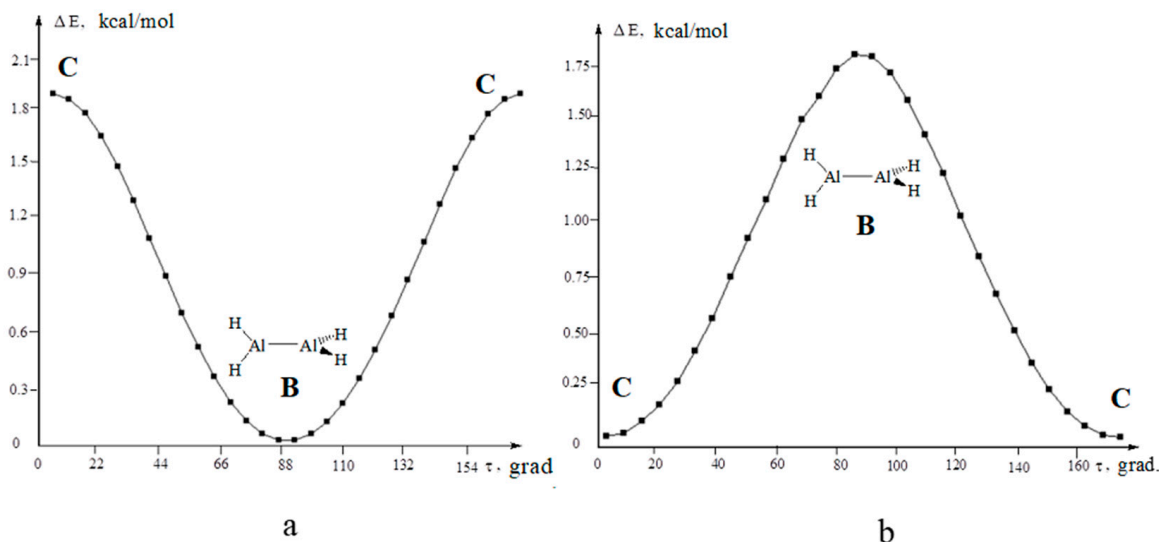**Figure 9.** Forms of dialane, Al_2H_4. Adapted with modification [178].

Figure 10. Relative energy of dialane Al_2H_4 as a function of the H–Al–Al–H torsion angle τ (0 K). (**a**) free molecule; (**b**) cluster Al_2H_4@(5,5). Adapted with modification [178].
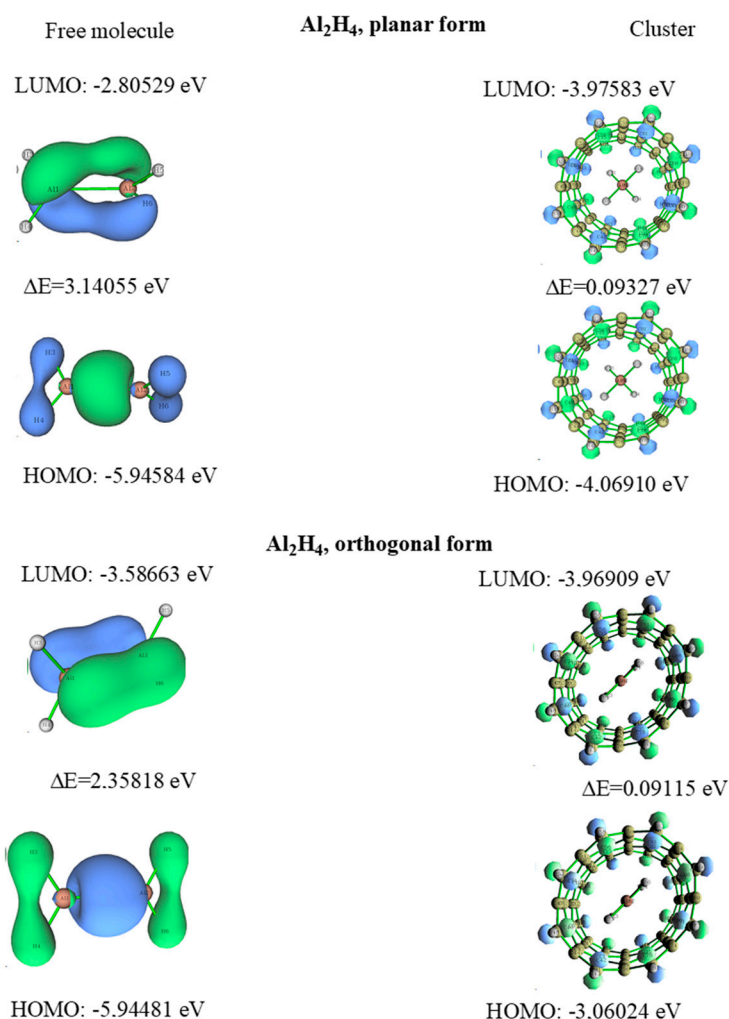
Figure 11. Differences in the energy of HOMO-LUMO of dialane (PBE/3ζ). Adapted with modification [178].

3.4. Hydrazine

Hydrazine, which is widely used in organic synthesis and in medicine, demonstrates the influence of unshared electron pairs on the rotation barrier about N–N bond. Its conformational equilibrium includes gauche-form **A** (global minimum), staggered form **B** (local TS) and eclipsed form **C** (main TS); the torsion angle τ in conformer **A** equals 91.5° [179–182]. The energy differences between conformations **A-B** and **A-C** ($\Delta G_{298}{}^{\neq}$) are 1.8 kcal/mol and 7.9 kcal/mol respectively (PBE/3ζ, Scheme 1) [183].
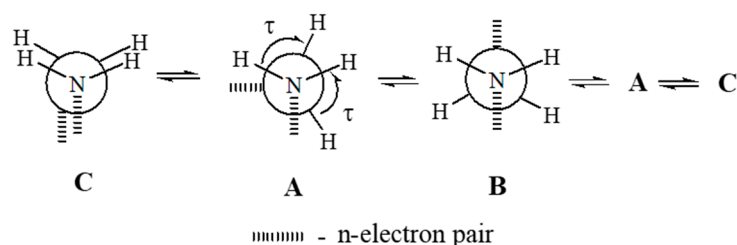
Scheme 1. Forms (**A**–**C**) of hydrazine.

The force field of SWCNTs substantively changes the conformational behavior of guest molecule (PBE/3ζ) [183]. Clusters N_2H_4@(4,4) demonstrate a significant decline (to 4.6 kcal/mol) of $\Delta G_{298}{}^{\neq}$ (forms **A-C**). In the case of SWCNTs (4,4) and (6,0), the main minimum of hydrazine belongs to the conformer **B** with $\Delta G_{298}{}^{\neq}$ **B-C** 1.1–2.2 kcal/mol. The increase in the diameter of the nanotube, as for

endocomplex N_2H_4@(6,6), results in an equilibrium close to the free hydrazine. In all cases, the guest molecule has a positive or negative electric charge [183].

3.5. Methanol and Methanethiol

Methanol and methanethiol are characterized by a hindered rotation with the potential barrier between gauche (**A**, minimum) and eclipsed (**B**, TS) forms at 1.07 and 1.27 kcal/mol respectively (Figure 12) [94,184]; according to PBE/3ζ approximation, the appropriate $\Delta G_{298}^{\neq}$ values are 1.0 and 1.2 kcal/mol [128,185]. However, in the cavity of SWCNT (6,0), their conformational behavior has significantly changed.
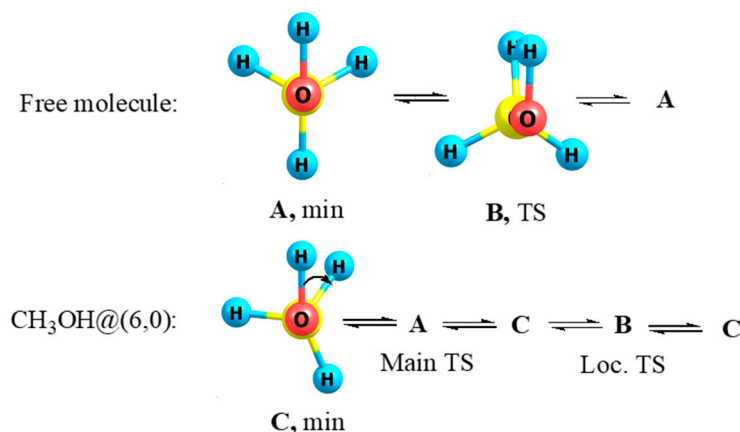

Figure 12. Conformational equilibrium of methanol. Adapted with modification [185].

In the case of cluster CH_3OH@(6,0), minimum on the PES belongs not to the form **A**, which becomes the main TS, but to the conformer **C,** with a torsion angle of HOCH 26.4° (PBE/3ζ, Figure 12). The main (**A**) and a local (**B**) TS are less stable by 0.27 and 0.03 kcal/mol respectively ($\Delta G_{298}^{\neq}$) [185]. Endocluster CH_3SH@(6,0) is characterized by the torsion angle HSCH 22.2° and $\Delta G_{298}^{\neq}$ values for **A** and **B** forms of 2.1 and 0.6 kcal/mol. In both cases, the guest molecule has a positive electric charge (0.3–0.7). Again, as in the previous examples, all this indicates the important role of *n*-electron pairs in the guest molecule, affecting changes in its conformational preference outside and inside nanotubes.

3.6. Dimethyl Ether

The molecule $(CH_3)_2O$ belongs to the systems with two internal rotors; the experimental barrier of rotation between **A** and **B** forms is 2.60 kcal/mol (near 900 cm^{-1}) (Figure 13) [186–189]. The origin and nature of the barrier, in particular the role of lone pairs, is widely discussed in the literature [190–193]. However, in the SWCNT cavity, the conformational behavior of this compound is significantly changed. In clusters $(CH_3)_2O$@(4,4), form **A** is not realized: during the optimization it converts to the unusual conformer **C**, which corresponds to the minimum and cannot exist outside the tube, turning back into form **A** (Figure 13) [194]. According to the PBE/3ζ, approximation the valence angle COC in the free molecule of dimethyl ether (form **A**) is 111.2°, which is very close to the experimental value (111.5° [188]). However, for form **C** in cluster $(CH_3)_2O$@(4,4), it rises to 127–130° [194]. Meanwhile, form **B** in this case also corresponds to the TS; the value of $\Delta G_{298}^{\neq}$ **B-C** (1.3–1.9 kcal/mol) is lower than that for the transition **A-B** of the free molecule (2.5 kcal/mol).

In the case of endocomplex $(CH_3)_2O$@(6,0), the angle COC in conformer **C** rises to 180° and the molecule takes the form of a rod with an eclipsed conformation of methyl groups (Figure 13). The appropriate transition state corresponds to the rod-shaped form, with a staggered conformation of methyl groups and $\Delta G_{298}^{\neq}$ 3.5 kcal/mol.

In all cases, the guest molecule has positive or negative charge and shortened C-O bonds [194].
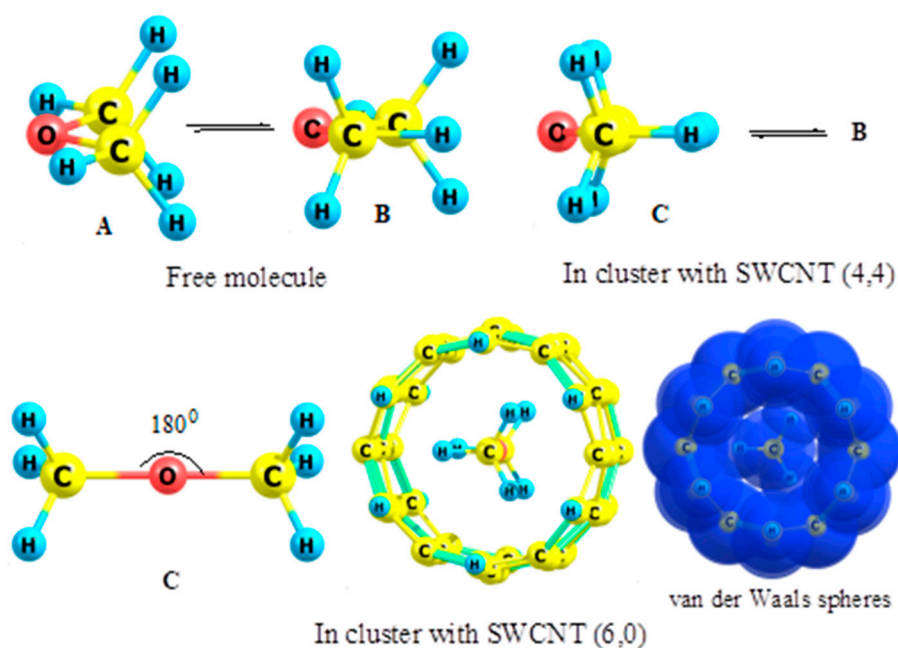
Figure 13. Conformations of dimethyl ether in the free state and in clusters with SWCNTs. Adapted with modification [194].

4. Conformational Properties of Simple Molecules in Fullerenes

4.1. Ethane and Its Analogs

The conformational behavior of ethane inside fullerenes of small diameter was studied on the example of cluster $C_2H_6@Si_{20}$ [195]. PES, in this case, contains tree stationary points: partially eclipsed **A** (global minimum), eclipsed **B** (main TS) and staggered **C** (local TS) (Figure 14).
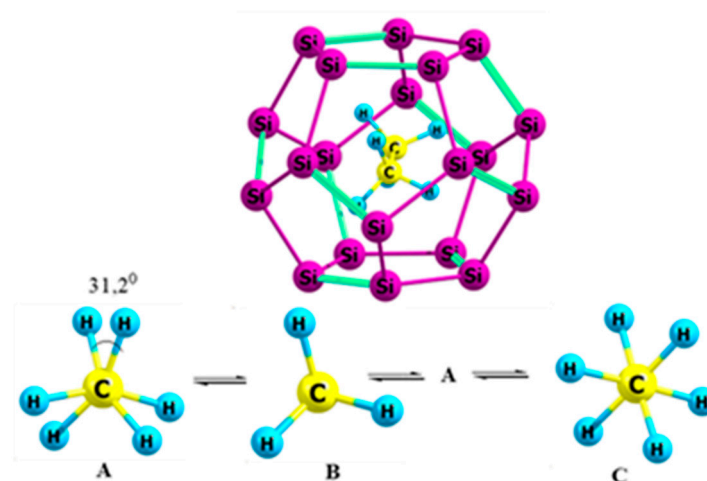

Figure 14. Conformational equilibrium of the guest molecule in cluster $C_2H_6@Si_{20}$. Adapted with modification [195].

Differences in energy between these forms ($\Delta G_{298}^{\neq}$, PBE/3ζ) account for 1.2 (**A-B**) and 0.4 (**A-C**) kcal/mol. Hence, compared to the free ethane, the internal rotation barrier has become two times lower. The guest molecule possesses a strong positive electric charge (1.3–1.4) and is characterized by shortened C–C bond length and a decline in its Mulliken bond order [195].

Endoclusters of ethane-like molecules with fullerenes C_{60}, C_{70}, C_{80} and their heteroanalogs, in contrast to the previous example, are characterized by only two stationary points on the PES:

staggered and eclipsed forms. The first corresponds to the minimum and the second to the TS [196–202]. Ethane inside the C_{60} cavity exhibits a higher barrier of internal rotation and shorter C–C bond length in comparison with the free molecule [196]. The same is true of its analogs; in some cases, the height of the barrier grows by more than threefold (Table 3). This increase in diameter of fullerenes (C_{60}, C_{70}, C_{80} and Si_{60}) naturally leads to the decrease in $\Delta G_{298}^{\neq}$. In the case of B-N fullerenes (their peculiarities have been discussed in [131]) this dependence is more mixed. In particular, in a series of endocomplexes, $C_2F_6@C_{60}$, $C_2F_6@C_{12}B_{24}N_{24}$ and $C_2F_6@B_{36}N_{24}$, the value of $\Delta G_{298}^{\neq}$ initially decreases and then increases, while it is still lower than that of the C_{60} cluster [198]. This influence of chemical composition is also valid for the $H_3B{\leftarrow}NH_3$ endocomplexes with fullerenes containing both 60 and 80 atoms in their shells [201]. Meanwhile, in series of C_2F_6 clusters with 80-atomic fullerenes, the barrier for the $(BNC)_{80}$ system is, vice versa, higher than those of C_{80} and $(BN)_{80}$ complexes (Table 3). All guest molecules have electric charge; in the case of C_5H_{12} clusters, it is rather large and changes the sign for different fullerenes [200]. Mulliken bond order for the central bond (O), with the exception of several $H_3B{\leftarrow}NH_3$ endocomplexes, depends little on the size and chemical composition of the fullerenes.

Table 3. Energetical and structural parameters of ethane and its analogs in fullerenes (PBE/3ζ).

Cluster; $\Delta G^{\neq}_{298}$ (kcal/mol) [1]	$r_{C–C}$ (Å) [1]	O [1]	Charge	Reference
$C_2H_6@C_{60}$; 3.3 (2,5)	1.465 (1.531)	1.12 (1.00)	−0.47	[196]
$C_2F_6@C_{60}$; 15.1 (4,6)	1.374 (1.565)	0.86 (0.88)	0.20	[197,198]
$C_2F_6@C_{12}B_{24}N_{24}$; 6.5	1.405	0.83	0.46	[198]
$C_2F_6@B_{36}N_{24}$; 8.2	1.464	0.86	0.48	[198]
$C_2F_6@C_{80}$; 7.2	1.477	0.89	−0.27	[197,198]
$C_2F_6@C_{14}B_{33}N_{33}$; 10.0	1.493	0.90	0.15	[198]
$C_2F_6@B_{47}N_{33}$; 7.6	1.507	0.92	0.15	[198]
$C_2Cl_6@C_{80}$; 43.5 (13,8)	1.431 (1.590)	0.98 (1.06)	−0.22	[199]
$C_5H_{12}@C_{60}$; 10.7 (3,8)	1.366 (1.539)	0.86 (1.00)	2.07	[200]
$C_5H_{12}@C_{80}$; 8.3	1.459	0.86	−1.27	[200]
$H_3B{\leftarrow}NH_3@C_{60}$; 4.4 (2,0)	1.522 (1.652)	0.43 (0.65)	−0.71	[201]
$H_3B{\leftarrow}NH_3@C_{12}B_{24}N_{24}$; 1.5	1.544	0.54	−0.79	[201]
$H_3B{\leftarrow}NH_3@B_{36}N_{24}$; 2.3	1.558	0.48	−0.22	[201]
$H_3B{\leftarrow}NH_3@C_{70}$; 2.1	1.595	0.62	−0.90	[201]
$H_3B{\leftarrow}NH_3@B_{41}N_{29}$; 1.8	1.610	0.72	−0.11	[201]
$H_3B{\leftarrow}NH_3@C_{80}$; 1.8	1.601	0.58	−0.64	[201]
$H_3B{\leftarrow}NH_3@C_{14}B_{33}N_{33}$; 1.1	1.605	0.57	−0.11	[201]
$H_3B{\leftarrow}NH_3@B_{47}N_{33}$; 1.6	1.618	0.64	−0.06	[201]
$Si_2H_6@Si_{60}$; 1.0 (1,3)	2.351 (3.355)	0.97 (1.00)	−0.12	[202]
$Si_2H_6@C_{80}$; 2.4	2.184	1.52	−1.16	[202]
$Si_2H_6@B_{47}N_{33}$; 1.6	2.252	1.08	0.01	[202]

[1] Values in round brackets correspond to the parameters for the free molecules ($r_{C–C}$, O and charge were given for the staggered form).

4.2. Methanethiol

The conformational equilibrium of methanethiol in endocomplexes with fullerenes, as for the free molecule, is characterized by gauche (minimum) and eclipsed (TS) forms (see part 3.5). But the height of the rotational barrier about the C-S bond ($\Delta G_{298}^{\neq}$), in this case, is increased: 2.0 and 2.7 kcal/mol for

the clusters $CH_3SH@C_{60}$ and $CH_3SH@C_{80}$, respectively, in comparison with 1.2 kcal/mol for the free molecule (PBE/3ζ) [203]. As in previous cases, the guest molecule has a certain electric charge (−0.5).

5. Conformational Behavior of Saturated Cyclic Molecules inside Nanotubes and Fullerenes

There are very few examples devoted to the behavior of saturated cyclic molecules, in particular, cyclohexane [33] and octasiloxane [27], inside SWCNTs. These are largely focused on the orientation of the guest molecule as a whole in the nanocavity. It should be noted, however, that in view of the structural transformations of acyclic molecules that were discussed in previous sections, the conformational behavior of cyclic systems inside nanoobjects also has a number of distinguishing features.

5.1. Cyclohexane in Nanotubes

It is well known that, at usual temperatures, molecules of cyclohexane exist in conformational equilibrium between chair (C, main minimum) and twist (Tw, local minimum) forms; the TS corresponds to the half-chair conformation (Scheme 2) [94].

C TS   *Tw*
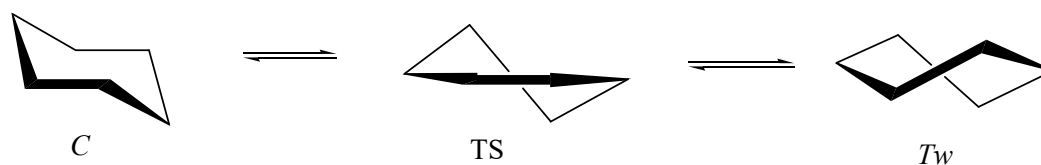
Scheme 2. Conformational equilibrium of free cyclohexane.

The conformational behavior of cyclohexane in the SWCNT cluster $C_6H_{12}@(8,0)$ is characterized by the absence of a Tw-form: the C-conformer directly converts into its invertomer C* over TS that corresponds to the conformation close to the flattened semi-planar form; the height of the barrier ($\Delta G_{298}^{\neq}$, PBE/3ζ, 10.4 kcal/mol) is very similar to that for the free cyclohexane (10.5 kcal/mol). The guest molecule has a positive charge (0.62) and is oriented in the direction perpendicular to the axis of the nanotube [204] (Figure 15).
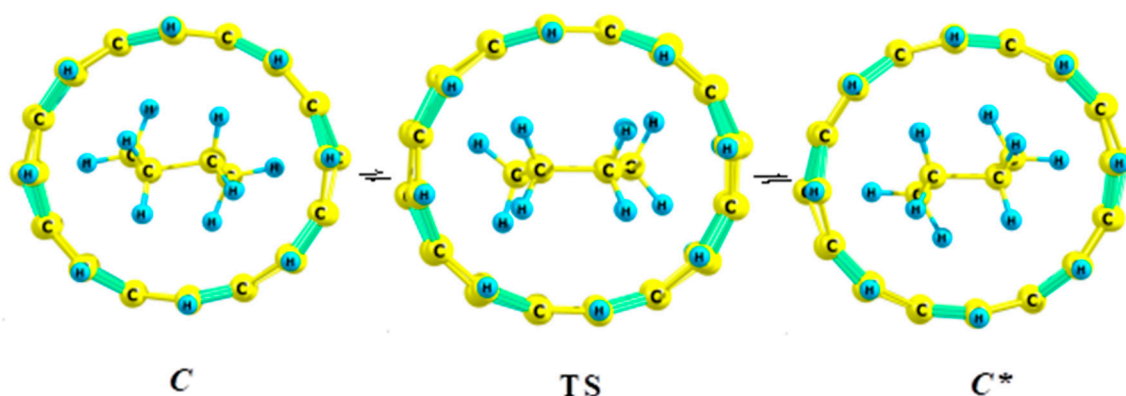

C T S $C*$

Figure 15. Conformational equilibrium of cyclohexane in cluster $C_6H_{12}@(8,0)$. Adapted with modification [204].

The conformational behavior of cyclohexane in cluster $C_6H_{12}@(5,5)$ is the same, except that TS in this case corresponds to the Tw-form, the height of the barrier is 6.8 kcal/mol and the guest molecule has a negative charge (−0.50) [204].

5.2. 1,3-Dioxane in Nanotubes

It is known that 1,3-dioxanes—very attractive heteroanalogs of cyclohexane—belong to the classical objects of conformational analysis [94]. Besides that, due to their wide range of pharmacological

action, they may be used for the creation of new drugs [205,206] and also as reagents in fine organic synthesis [207–211]. All this makes it relevant to consider the conformational properties of these compounds inside nanotubes, from the perspectives of nanoreactors [68–75] and drug delivery systems [15,19].

The PES of unsubstituted 1,3-dioxane, $C_4H_8O_2$, contains tree minima (C—the main, 2,5-Tw and 1,4-Tw-forms—the local) (Scheme 3) [94,212].
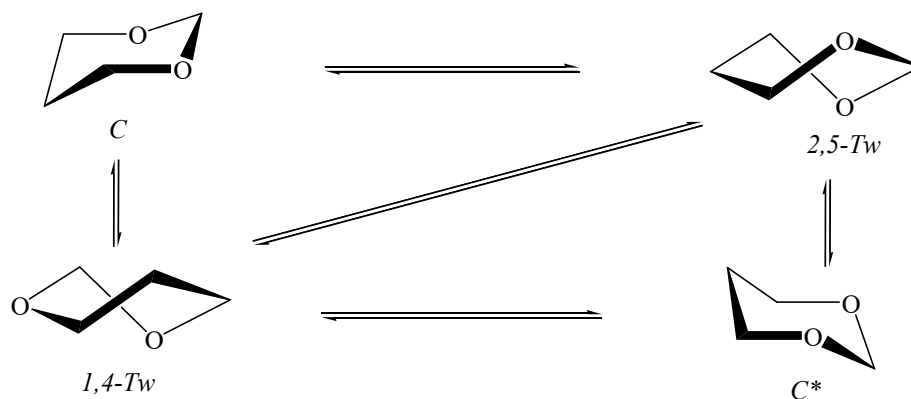
Scheme 3. Conformational equilibrium of free 1,3-dioxane.

However, in a SWCNT cavity of small diameter (≤8.4 Å), the relative population of these forms significantly changes. In the case of cluster $C_4H_8O_2$@(6,6), the 1,4-Tw conformer is not realized, and PES contains only C (main minimum) and 2,5-Tw-forms with ΔG_{298}^0 3.1 kcal/mol, which is significantly lower than for free 1,3-dioxane (5.0 kcal/mol). In the case of clusters $C_4H_8O_2$@(5,5) and $C_4H_8O_2$@(8,0), the main minima correspond to the 2,5-Tw-conformer, and are 3.0 and 0.3 kcal/mol, respectively, more stable than the C-form; the last remains only as a local minimum. At the same time, the barrier of interconversion ($\Delta G_{298}^{\neq}$) is reduced by up to 5.1 kcal/mol in comparison with 9.7 kcal/mol for free 1,3-dioxane (PBE/3ζ) [213]. Cluster $C_4H_8O_2$@(7,0) demonstrates the presence of only one form—2,5-Tw; the C-conformer in this case is not realized (Figure 16). The van der Waals spheres show that the inner cavity of the nanotube is densely filled with 1,3-dioxane. In all cases, the guest molecule has a negative electric charge.
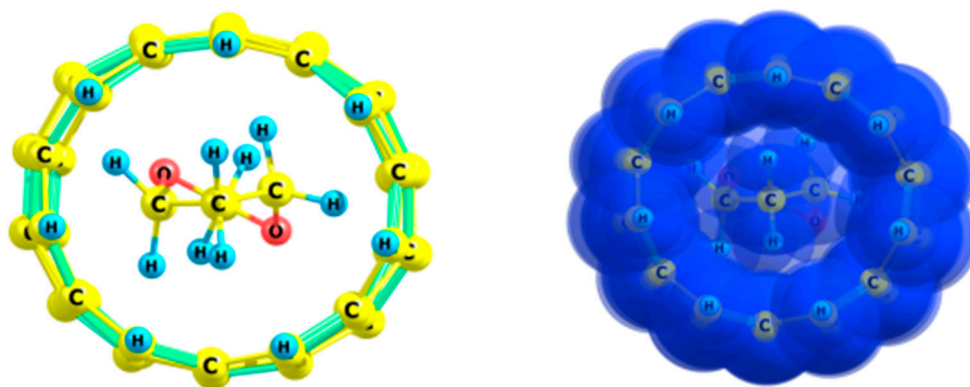

Figure 16. Cluster $C_4H_8O_2$@(7,0). Adapted with modification [213].

It should be stressed that the conformational behavior of substituted 1,3-dioxanes in usual solvents is not accompanied by the inversion of stability between the chair and any other form; in all cases, C-conformer remains the main minimum, and the role of the medium is relegated only to the shift of the conformational equilibrium towards the chair-form with more or less polarity, due to the axial or equatorial orientation of polar substituents or with lower steric restriction [214,215]. In sharp contrast,

the conformational properties of unsubstituted 1,3-dioxane in the SWCNT cavity are caused by the action of a new driving force, which can dramatically alter conformational properties of the guest cyclic molecules in comparison with those in the gas phase or in the usual solvents.
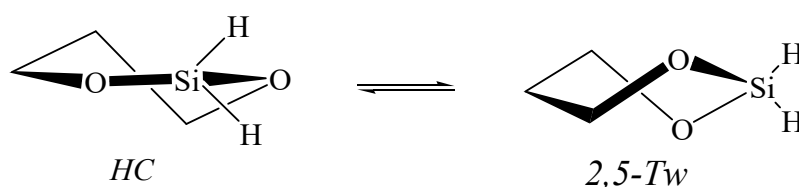
5.3. 1,3-Dioxa-2-Silacyclohexane in Nanotubes

The stereochemistry of silicon-containing saturated heterocycles is an integral part of organosilicon chemistry; the introduction of silicon atoms changes the geometry and electronic features of the cyclic system [216]. According to the results of gas-phase electron diffraction, the molecular structure of 2,2-dimethyl-1,3-dioxa-2-silacyclohexane corresponds to the flattened chair [217]. Theoretical investigation using Hartree–Fock (HF) and DFT approximations led to the conclusion of a rather low barrier of interconversion between two C-forms, including a local minimum of 2,5-Tw, which is very close in energy to the TS (Scheme 4) [212,217–219]. In the case of free 1,3-dioxa-2-silacyclohexane, $C_3H_8SiO_2$ (R=H), the corresponding $\Delta G_{298}^{\neq}$ is 4.1 kcal/mol (PBE/3ζ) [220].
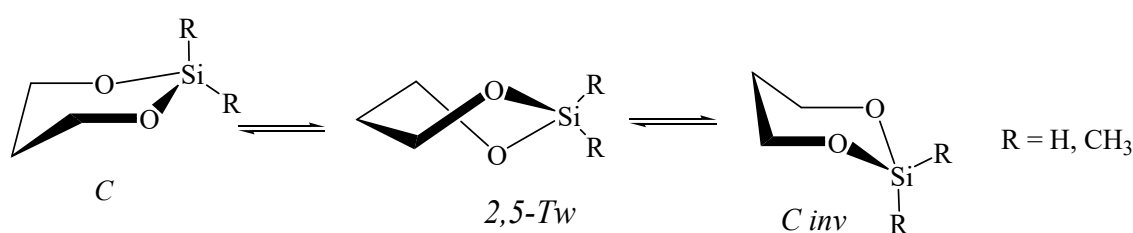
Scheme 4. Conformational equilibrium of free 1,3-dioxa-2-silacyclohexane.

It was found that the main minimum of the guest molecule in cluster $C_3H_8SiO_2@(5,5)$ belongs to the structure close to the half-chair (CH) conformer, not to the C-form. But other than that, the details of conformational behavior of encapsulated molecule remain the same; the barrier of interconversion is slightly higher than for the free molecule (5.1 kcal/mol, Scheme 5). Form 2,5-Tw remains the local minimum on the PES [220].

Scheme 5. Conformational equilibrium of 1,3-dioxa-2-silacyclohexane inside SWCNT (5,5).

In the case of cluster $C_3H_8SiO_2@(8,0)$ the main minimum corresponds to the C-conformer. Equilibrium C ↔ 2,5-Tw in this case is described by the relatively low energy differences between these forms (2.6 kcal/mol in comparison with 3.3 kcal/mol for the free silicon ester and previous cluster). The barrier of interconversion is slightly increased (4.8 kcal/mol). In all cases the guest molecule has a negative electric charge (−0.25–−0.87) [220].

Thus, SWCNTs cavity may change the conformation corresponding to the minimum as well as alters certain energy characteristics of conformational equilibrium of six membered cyclic silicon esters.

5.4. Hexahydropyrimidin-2-One in Nanotubes

Substituted hexahydropirimidine-2-ones belong to the promising class of cyclic urea derivatives with a well-defined biological activity [221] and as reagents in organic chemistry [222,223]. According to the X-ray investigation their structure corresponds to the semi-planar form, or C-conformer with a strong flattened heteroatomic part [224]. Conformational transformation of the free molecule of hexahydropyrimidin-2-one, $C_4H_8N_2O$, established by HF/6-31G(d) and PBE/3ζ methods includes two

degenerated in energy flattened C-conformers, 2,5-Tw as a local minimum and TS that corresponds to the conformation very close in energy to the 2,5-Tw form (Scheme 6) [225,226].
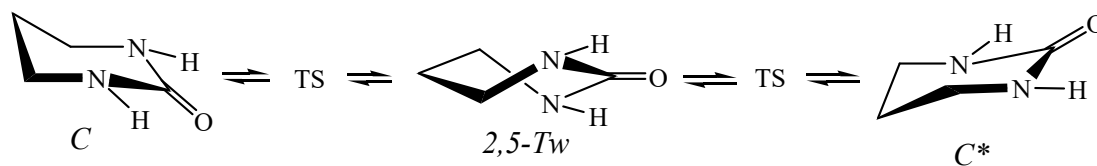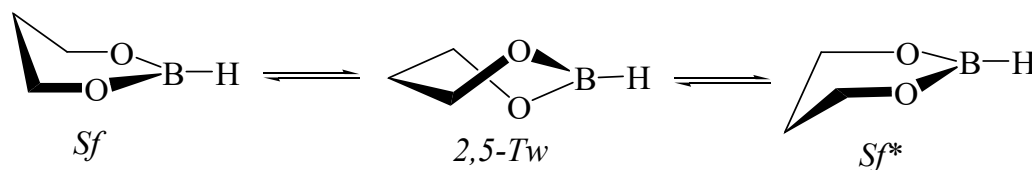

Scheme 6. Conformational equilibrium of free hexahydropirimidine-2-one.

Conformational equilibrium of hexahydropirimidine-2-one in cluster $C_4H_8N_2O@(5,5)$ exhibits the absence of 2,5-Tw form as a local minimum: it becomes a TS. Besides this conformation PES contains two degenerated in energy flattened C-forms with the increased barrier of interconversion (5.4 kcal/mol in comparison with 3.3 kcal/mol for the free cyclic urea, PBE/3ζ). The guest molecule acquires a negative electric charge (−0.66). In the case of cluster $C_4H_8N_2O@(8,0)$ PES besides C-form and TS includes 2,5-Tw conformer as a local minimum; the value ΔG_{298}^0 between them (3.1 kcal/mol) is higher than for the free molecule (2.4 kcal/mol), but the barrier of interconversion (3.5 kcal/mol) changes very little. The encapsulated molecule has a positive charge (0.32) [226].

Thus, the influence of nanotubes on the conformational properties of unsubstituted cyclic urea is down mainly to the qualitative change in the nature of intermediate forms and to the variation in energy parameters of conformational equilibrium between flattened C-conformers.

### 5.5. 1,3,2-Dioxaborinane in Fullerenes

It was established recently that preferable conformation of 1,4-dioxane in exo adducts with C_{60} and C_{70} fullerenes is not a chair but a boat form. Such unusual result is connected with a rigidity of fullerene skeleton [227]. In this connection it would be interesting to assess the conformational properties of the guest cyclic molecule inside fullerenes. The first example of its kind was the simplest six-membered cyclic boronic ester: 1,3,2-dioxaborinane. It belongs to the valuable class of organoboron compounds which are widely used in organic syntheses [228–231] and are convenient models to assess the effect of heteroatoms in changing of the conformational properties of cyclohexane's heteroanalogs [212]. The PES of 1,3,2-dioxaborinane itself ($C_3H_7BO_2$) contains degenerated in energy conformers of sofa (Sf) and TS—2,5-Tw form (Scheme 7) [212].

Scheme 7. Conformational equilibrium of free 1,3,2-dioxaborinane.

It should be noted that stabilization of Sf-form in the free molecule is due to the p-π conjugation in the heteroatomic part of the cyclic ester because of the partially double nature of B-O bond [212]. However, endocomplex $C_3H_7BO_2@C_{80}$ demonstrates the conformational equilibrium between two unusual for this class of compounds boat (B) forms with $\Delta G_{298}^{\neq}$ 10.1 kcal/mol in comparison with 7.2 kcal/mol for the free molecule of cyclic boronic esters (PBE/3ζ, Scheme 8); the guest molecule has a negative charge (−0.74) [232].

The decrease in fullerene diameter leads to the more significant changes in conformational properties of the guest molecule. In cluster $C_3H_7BO_2@C_{60}$ the main minimum on the PES of cyclic ester belongs to the 1,4-Tw form that may convert to the C-conformer (local minimum) over TS—envelop (E) form (Scheme 9).
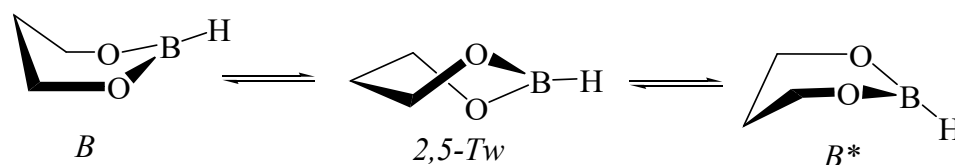
Scheme 8. Conformational equilibrium of 1,3,2-dioxaborinane in cluster $C_3H_7BO_2@C_{80}$.
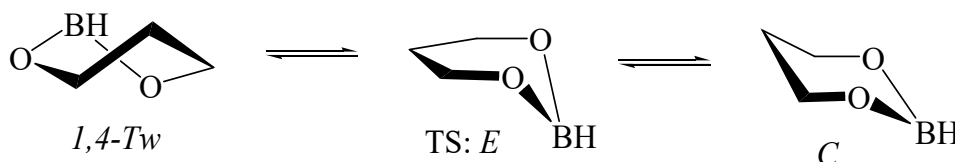
Scheme 9. Conformational equilibrium of 1,3,2-dioxaborinane in cluster $C_3H_7BO_2@C_{60}$.

The value ΔG_{298}^0 between 1,4-Tw and C-conformers is 8.1 kcal/mol and the height of the barrier is 27.9 kcal/mol (3.9 times higher than calculated for the free ester); the guest molecule acquires a large positive charge (2.53 for the 1,4-Tw form) [232].

Thus, a combination of electronic and steric requirements that may be called as a force field inside fullerenes significantly changes conformational properties of even relatively simple cyclic molecule: forms like B, 1,4-Tw, E and C are never realized for 1,3,2-dioxaborinanes with sp^2 boron atom in any solvent [212]. The sharp increase in population of twist-form is connected primarily with a considerable decline in linear size of the molecule inside fullerenes under the action of force field.

6. Nitrogen Pyramidal Inversion inside Nanotubes and Fullerenes

Recent years exhibit a significant interest to the investigation of pyramidal inversion in XH_3 compounds [233]. One of the main challenges facing the theoretical spectroscopy is connected with a selection of ab initio and DFT methods that can ensure the accurate estimate the energy of nitrogen inversion barrier [234]. Authors of [235] suggested a benchmark set that comprises 24 high-level wave-function inversion barriers in different compounds; it is submitted that at least medium-sized triple-split-valence basis sets with at least one set of polarization functions should be used for the theoretical study of pyramidal inversion. Formally, method PBE/3ζ [87,92] quite meets those criteria. It should be stressed however that it is also underestimates the nitrogen inversion barrier in amines.

How an ordinary solvent affects the barrier of nitrogen pyramidal inversion? It was established that in polar medium this value depends on the number of solvent's molecules in the close surroundings of the dissolved species. In particular, computer simulation of inversion in 3-methyltetrahydro-1,3-oxazine surrounded by the molecules of difluorodichloromethane using PBE/3ζ approximation (explicit model) revealed that the best match with experimental barrier was obtained for the case of four molecules in solvation shell [236].

6.1. Ammonia and Trimethylamine in Nanotubes

Experimental values of nitrogen pyramidal inversion barriers in ammonia and trimethylamine ($\Delta G_{298}^{\neq}$) are 5.8 and 7.5 kcal/mol respectively [237]. The appropriate results of PBE/3ζ has been understated (4.3 and 6.0 kcal/mol [238]). However, considering numerous challenges relating to the application of more complex methods and basis sets to the calculation of nanoobjects, it was possible to use the PBE/3ζ approach for the estimation of the inversion barrier of amines in SWCNTs. In the case of cluster $NH_3@(4,4)$ the value of $\Delta G_{298}^{\neq}$ was 10,9 kcal/mol (more than 2.5 times higher than for the free molecule). In contrast, the appropriate value for trimethylamine in cluster $N(CH_3)_3@(6,6)$ was 4.8 kcal/mol (1.25 times lower than for the free molecule) [238]. It should be noted that the distance between guest species and carbon skeleton of SWCNT in both cases was the same (~2.5 Å). Thus, the value of inversion barrier in nanotube's cavity as for the free molecule depends to some extent on the nature of amine. In both cases the guest molecule acquires a relatively small charge (up to −0.50).

6.2. Piperidine inside Nanotube

It is necessary to separate two dynamic processes relatively to piperidine ($C_5H_{11}N$): nitrogen pyramidal inversion and interconversion of the cycle. The first leads to the change in orientation of N-H proton (axial-equatorial, a–e) and the second over several steps—to the alternate conformation (Scheme 10) [239].
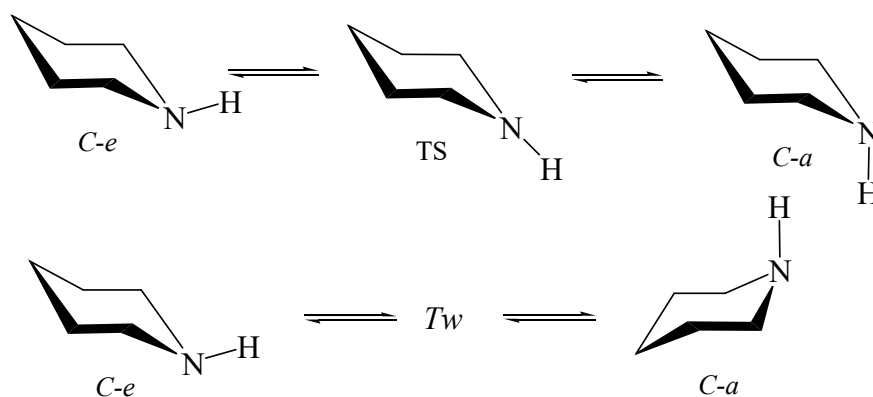

Scheme 10. Two ways of conformational transformation C-e ↔ C-a of free piperidine.

According to the NMR spectroscopy data the barrier of nitrogen pyramidal inversion ($\Delta G_{298}^{\neq}$) is 6.1 kcal/mol [240] and $\Delta G_{298}^{\neq}$ for the second process—10.4 kcal/mol [241]. So, the nitrogen inversion in this case requires lower energy compared to the conformational equilibrium of the cycle. Besides that, conformer C-e is more stable than C-a in the gas phase (0.72 kcal/mol) [242] and in nonpolar medium (0.2–0.6 kcal/mol) [243].

In cluster $C_5H_{11}N@(6,6)$ the barrier of nitrogen inversion rises to 6.8 kcal/mol in comparison with 4.7 kcal/mol for the free molecule (PBE/3ζ) [244]. At the same time form C-a becomes more stable inside SWCNT; differences with C-e conformer (ΔG_{298}^{0}) is 2.6 kcal/mol compared to 0.6 kcal/mol in favor of form C-e for the free molecule. The encapsulated piperidine acquires a relatively large negative charge (−0.89 for the C-a form) [244].

6.3. Perhydro-1,3,2-Dioxazine inside Nanotubes

Perhydro-1,3,2-dioxazine ($C_3H_7NO_2$) is the heteroanalog of cyclohexane with O–N–O ring fragment. It was firstly obtained 35 years ago [245]. Further study showed that this compound is conformationally rigid due to the relatively high barrier of nitrogen inversion in *N,N*-dialkoxyamines (21.7–24.6 kcal/mol) [246,247]. Detailed conformational analysis using MP2-RI/λ2 approximation revealed that the $\Delta G_{298}^{\neq}$ value for the direct transformation C-a ↔ C-e forms of perhydro-1,3,2-dioxazine is 23.3 kcal/mol (Scheme 11). Wherein conformer C-e is more stable at 2.5 kcal/mol (ΔG_{298}^{0}) [248].
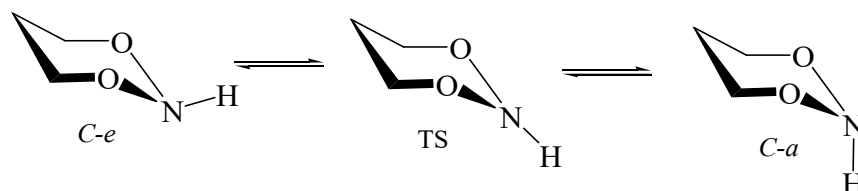
Scheme 11. Conformational equilibrium of free perhydro-1,3,2-dioxazine.

In contrast to the free molecule cluster $C_3H_7NO_2@(6,6)$ demonstrates the preference of C-a form (ΔG_{298}^{0} 2.1 kcal/mol, PBE/3ζ). The barrier of the nitrogen inversion is almost unchanged, compared to the free molecule ($\Delta G_{298}^{\neq}$ 23.4 and 21.7 kcal/mol respectively). The C-a form in the SWCNT cavity is slightly distorted [249]. The preference of C-a form is also observed in endocomplex $C_3H_7NO_2@(5,5)$;

the corresponding $\Delta G_{298}{}^0$ is 1.1 kcal/mol and $\Delta G_{298}{}^{\neq}$ for nitrogen inversion is rather close to the free perhydro-1,3,2-dioxazine (20.2 kcal/mol). In both cases the guest molecule acquires a positive charge (0.60–0.65) [249].

6.4. Ammonia and Trimethylamine in Fullerenes

Cluster $NH_3@C_{60}$ demonstrates almost the same barrier on nitrogen inversion as in the free molecule (4.4 kcal/mol); the N-H bond lengths remain practically unchanged and the guest molecule has a small negative charge (−0.30) [250]. Thus, the cavity of C_{60} is large enough to cause changes in the energy of inversion. In contrast, the inner space of fullerene in the case of $N(CH_3)_3@C_{60}$ becomes rather small: the height of the barrier in this case is 3.4 times higher than for the free molecule (25.7 kcal/mol); the C-N bond lengths became shorter by 0.08 Å and the guest molecule acquires a positive charge (0.65 for the ground state and 1.14 for the TS). The increase of fullerene's diameter leads to the decrease of $\Delta G_{298}{}^{\neq}$ for nitrogen inversion (10.3 kcal/mol for the cluster $N(CH_3)_3@C_{80}$); the molecule of amine in this case has a negative charge (−0.83 for the ground state and −0.36 for the TS) [250].

Thus, the pyramidal inversion barrier for acyclic amines inside nanotubes and fullerenes depends on the nature of amine and on the size of nanocavity. In the case of cyclic amines in SWCNTs the inversion of the relative stability of axial and equatorial conformers is observed and, in the case of pyrimidine, the barrier of the nitrogen pyramidal inversion is increased in 1.4 times.

7. Recognition of the R- and S-Isomers by Chiral Nanotubes

It is well known that helicity is closely linked to chirality, because left-handed and right-handed helixes are non-superimposable to their mirror images. A distinctive feature of chiral nanotubes is the presence of a helical axis. This class of SWCNTs can be described by (n,m) chirality indexes (n ≠ m; m ≠ 0). A different chirality suggests that such objects create the individual enantiomeric pairs, also denoted as P and M nanotubes with a single set of values (n,m) [251]. Depending on the ratio between chirality indexes, they display features of conductors or semiconductors [252] and have valuable optical properties [253]. It was shown that the doping of chiral nanotubes with nitrogen diminishes the stress caused by the small diameter and the corresponding energy strongly depends on the tube helicity [254]. However, the most prominent quality of chiral nanotubes is their ability to form complexes with chiral molecules possessing different degrees of stability. In principle, this enable to provide asymmetric synthesis [76] and make possible a separation of left-handed from right-handed isomers by using, for example, chiral SWCNTs as stationary phases in chromatography. It is also possible to induce chirality in the chains of guest molecules [251,255,256]. In this connection, the relative stability of some R- and S-isomers in the cavity of chiral nanotubes was investigated using the PBE/3ζ approximation.

7.1. R- and S-Isomers of 1-Fluoroethanol Inside SWCNTs (4,4) and (4,1)

According to the previous analysis, both enantiomers of free 1-fluoroethanol (C_2H_5FO) participate in conformational equilibrium between **a** and **b** forms with differences in stability ($\Delta G_{298}{}^0$) 0.3 kcal/mol in favor of **a** (Figure 17) [257]. This result is confirmed by [258].
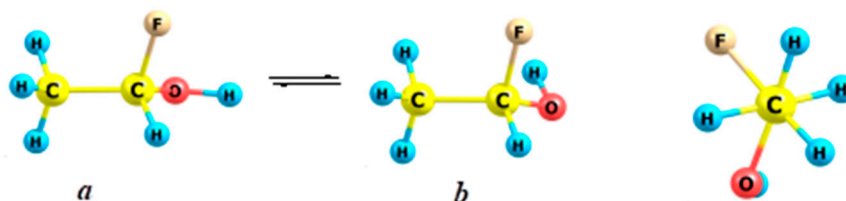

Figure 17. Conformers of S-1-fluoroethanol. Adapted with modification [257].

It should be noted that both nanotubes—(4,4) and (4,1)—that were used as nanoobjects in clusters with 1-fluoroethanol have the same gross formula ($C_{80}H_{16}$), but SWCNT (4,4) is more stable than (4,1) at 0.6 kcal/mol (ΔG_{298}^0). Hence, these nanotubes can be viewed as structural isomers.

Molecules of 1-fluoroethanol inside SWCNTs (4,4) and M(4,1) convert into preferable conformation close to the eclipsed (Figure 18).
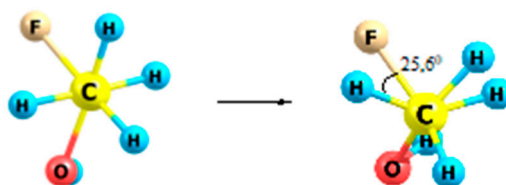

Figure 18. Preferred conformation of S-1-fluoroethanol inside SWCNTs. Adapted with modification [257].

The energies of clusters $R-C_2H_5FO@(4,4)$ and $S-C_2H_5FO@(4,4)$ were predictably the same. However, endocomplex $R-C_2H_5FO@M(4,1)$ was proven to be more stable than $S-C_2H_5FO@M(4,1)$ at 4.4 kcal/mol, and in comparison with cluster $C_2H_5FO@(4,4)$ at 12.8 kcal/mol (ΔG_{298}^0). This means that, despite the greater stability of SWCNT (4,4), cluster $R-C_2H_5FO@M(4,1)$ exhibits a large energy gain which can serve as a theoretical basis to separate both enantiomers. Besides that, the guest molecule in all cases has a slight negative charge (up to -0.12) [257].

7.2. R- and S-Isomers of α-Alanine inside SWCNTs (n,m)

Conformational analysis of free α-alanine ($C_3H_7NO_2$), carried out for S-isomer by rotating around the bond C(NH$_2$)–C(O), indicates the presence of several stationary points on the PES; the main minimum corresponds to the form **A**, and the main TS to the conformation **B** (Scheme 12, Table 4) [259]. These results are quite consistent with the data of [260].
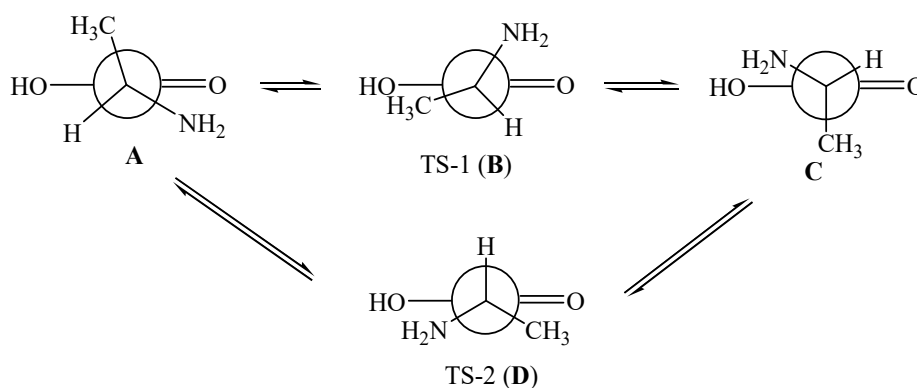
Scheme 12. Conformational equilibrium of free α-alanine.

SWCNTs (5,5), (5,1) and (5,2), which were used as nanoobjects for the investigation of α-alanine properties in endocomplexes, differ in energy: as in the previous case (Section 7.1), the most stable is nanotube (5,5) (Table 4).

The conformational behavior of α-alanine in clusters, for the example of $S-C_3H_7NO_2@P(5,2)$, is presented in Scheme 13. In this case, the main minimum on the PES corresponds to the conformer **D**.

Comparison of clusters' energy (Table 4) indicates that in a series of clusters with SWCNTs: (5,5), (5,1) and (5,2) their relative stability grows; the most stable are practically degenerated in energy endocomplexes $S-C_3H_7NO_2@P(5,2)$ and $R-C_3H_7NO_2@M(5,2)$ (Figure 19). Thus, the increase in chirality index m leads to a rise in the relative stability of the appropriate chiral clusters.

Table 4. Relative energies of SWCNTs, α-alanine and clusters of α-alanine together with the electric charge of the guest molecule (PBE/3ζ) [259].

Object	$\Delta G_{298}{}^0$ ($\Delta G_{298}{}^{\neq}$), kcal/mol	Electric Charge
(5,5)	0	0
P,M(5,1) [1]	5.9	0
P,M(5,2) [1]	16.1	0
S-$C_3H_7NO_2$ (**A**)	0	0
S-$C_3H_7NO_2$ (**B**) [2]	(3.1)	0
S-$C_3H_7NO_2$ (**D**) [2]	(2.7)	0
R,S-$C_3H_7NO_2$@(5,5) [3]	13.9	−0.69
S-$C_3H_7NO_2$@M(5,1) [3]	12.3	−0.69
S-$C_3H_7NO_2$@P(5,1) [3]	12.1	−0.67
R-$C_3H_7NO_2$@M(5,1) [3]	12.1	−0.67
R-$C_3H_7NO_2$@P(5,1) [3]	12.3	−0.69
S-$C_3H_7NO_2$@M(5,2) [3]	4.6	−0.64
S-$C_3H_7NO_2$@P(5,2)	0	−0.67
R-$C_3H_7NO_2$@M(5,2) [3]	0.1	−0.67
R-$C_3H_7NO_2$@P(5,2) [3]	4.7	−0.65

[1] Relative to (5,5). [2] Relative to form **A**. [3] Relative to S-$C_3H_7NO_2$@P(5,2) (conformer **D** for α-alanine).
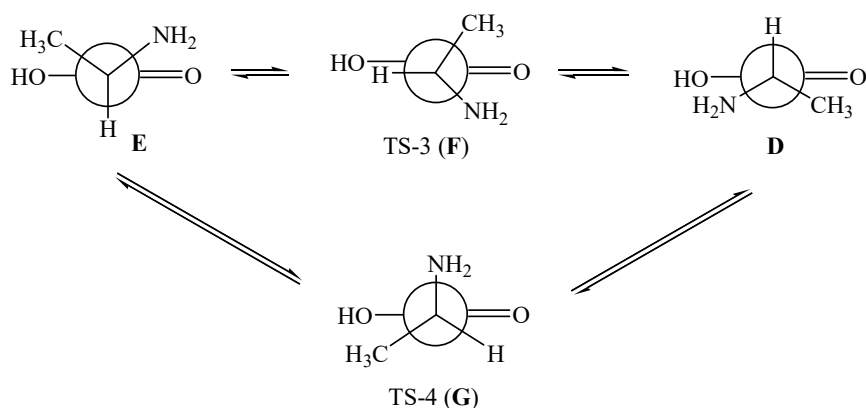
Scheme 13. Conformational equilibrium of S-$C_3H_7NO_2$@P(5,2).
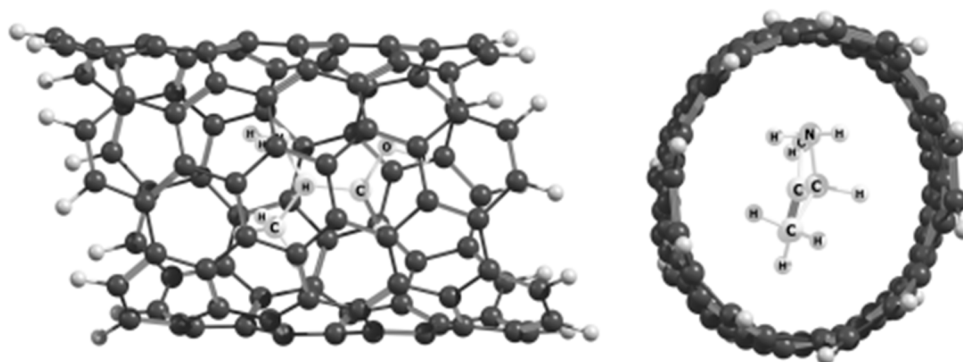
Figure 19. The most stable endocomplex, S-$C_3H_7NO_2$@P(5,2). Adapted with modification [259].

All results confirm the earlier conclusion [257] that the combination of S-enantiomer with P-SWCNT and R-enantiomer with M-SWCNT leads to the formation of most stable endocomplexes and creates a theoretical foundation for the recognition and effective separation of optical isomers.

8. Relative Stability of Cis and Trans Isomers inside Nanotubes. The "Trans-Effect"

It is well known that, in some cases, the cis isomer of compounds with a double bond is more stable than its trans form. This applies, for example, to 1,2-difluoroethene and difluorodiazene [261,262]. Such phenomenon is called the "cis effect", and its probable causes have been discussed in the literature [263–266]. In particular, according to [266], the cis effect in the case of difluorodiazene is caused for a number of reasons. One of them is connected with a destabilization of the trans form because of the increased ionic character of the bonds linking the central to the peripheral atoms. This leads to the destabilizing reduction of the valence angles in both isomers, but in cis form this change is relaxed by Coulombic repulsion between two terminal atoms.

Using the PBE/3ζ approximation, it has been shown that free 1,2-difluoroethene and difluorodiazene demonstrate an advantage in energy in their cis form. However, investigation of the relative stability of both isomers in the cavity of SWCNT (4,4) demonstrates the action of the "trans-effect": the predominance of the trans-configuration. The energy differences from the cis form reach two-digit numbers (Table 5) [267,268]. The same pattern is valid also for the cluster CHF=CHF@(6,6), although with less distinction in energy between both isomers.

Table 5. Relative energies of geometric isomers of 1,2-difluoroethene and difluorodiazene, their endocomplexes with SWCNTs, the bond order of the double bond, $O_{X=X}$ and the electric charge on the guest molecule (PBE/3ζ) [267,268].

Object	ΔG_{298}^0, kcal/mol	$O_{X=X}$	Charge
CHF=CHF, *cis-*	0	1.78	0
trans-	0.6	1.77	0
FN=NF, *cis-*	0	1.76	0
trans-	3.4	1.66	0
CHF=CHF@(4,4), *cis-*	26.2	1.32	0.46
trans-	0	1.44	0.52
CHF=CHF@(6,6), *cis-*	0.9	1.72	−0.16
trans-	0	1.73	−0.17
FN=NF@(4,4), *cis-*	27.4	1.46	−0.36
trans-	0	1.73	−0.36
FN=NF@(6,6), *cis-*	0	1.71	−0.03
trans-	3.8	1.69	−0.004

The observed effect depends on the diameter of the nanotubes (Figure 20). It should be noted that there are several reasons for this complex phenomenon. On the one hand, the force field inside the nanotube significantly changes the structure of the guest species. In particular, the distance between fluorine atoms in cis-N_2F_2@(4,4) (2.402 Å) is shorter than for the free cis-difluorodiazene (2.452 Å), which enhances additional internal stress and leads to the destabilization of cis-configuration. On the other hand, in the case of cis-CHF=CHF@(4,4), the observed distance (3.084 Å) becomes greater than for the free cis-1,2-difluoroethene (2.793 Å). However, the cis isomer still remains unstable. Hence, it is also necessary to take into account the role of electronic factors: the noticeable change in Mulliken bond order ($O_{X=X}$, Table 5) inside SWCNT (4,4) demonstrates a significant redistribution of electron density in the guest molecule, probably because of orbital interactions with the π-system of the nanotube.

Thus, SWCNTs are able to drastically change the relative stability of cis and trans isomers in their cavity for several reasons.
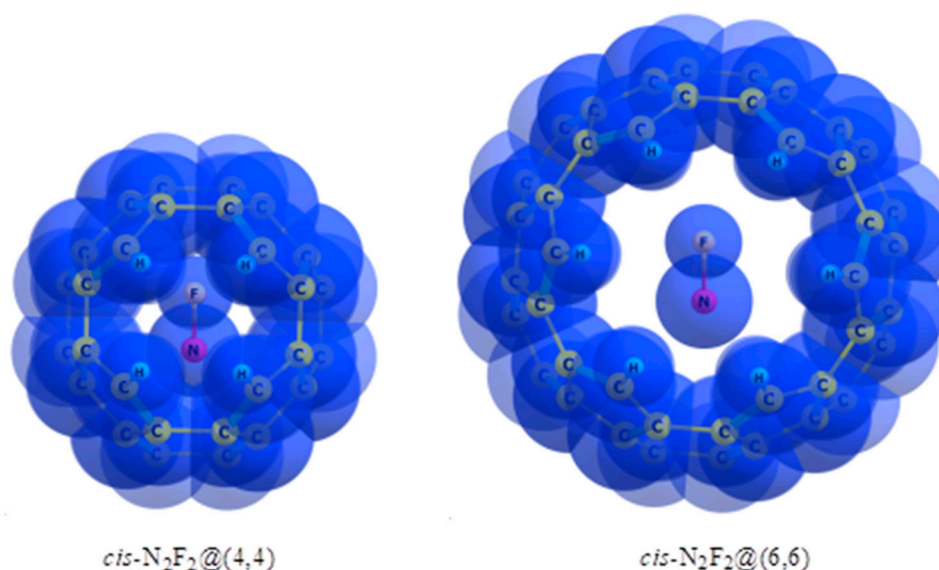
$cis\text{-}N_2F_2@(4,4)$ $cis\text{-}N_2F_2@(6,6)$

Figure 20. Clusters of cis-N_2F_2 in the light of van der Waals spheres. The distances between the guest molecule and the SWCNT wall are 2.4 Å and 3.7 Å for (4,4) and (6,6) endocomplexes, respectively. Adapted with modification [267].

9. Conclusions

Promising opportunities of different nanostructured objects are largely connected with the formation of endohedral complexes of fullerenes and nanotubes. Unique conditions in their cavities can be viewed as the action of a solvent with specific properties. As a result, a combination of electronic and steric requirements, that may be called a force field, inside fullerenes and nanotubes significantly changes the stereochemical properties of even relatively simple molecules in comparison with their free state or with the action of usual solvents. Principal differences are mainly the following:

- The preferred conformation of ethane and its analogs inside nanotubes of small diameter is not the staggered, but the eclipsed form. The conformational behavior of ethane-like molecules inside fullerenes is less clear and depends on the size and chemical composition of the nanoobject.
- Hydroxyborane and diborane in endohedral clusters of nanotubes are characterized by reducing the barriers of internal rotation about the B-O and B-B bonds; in the case of dialane, the planar form—the transition state for the free molecule—becomes the minimum on the potential energy surface. A similar change in the nature of the preferred conformation is observed for hydrazine, methanol, methanethiol and dimethyl ether, together with cyclic molecules: cyclohexane, 1,3-dioxa-2-silacyclohexane and hexahydropirimidine-2-one inside nanotubes. In the case of 1,3-dioxane inside SWCNT and 1,3,2-dioxaborinane inside fullerene C_{60} conformational equilibrium is shifted to forms that can never be realized as a ground state for neither free molecule, nor for these species in any solvent.
- The barrier to pyramidal inversion of amines in endocomplexes varies depending on the nature of the amine and the size of the nanocavity.
- Chiral nanotubes are able to recognize molecules of enantiomers owing to increased affinity of *P*-SWCNT for the *S*-isomer and *M*-SWCNT for the *R*-form.
- SWCNTs of small diameter are able to drastically change the relative stability of cis and trans isomers in their cavity.

Everything mentioned above indicates fundamental changes in the structural properties of the guest species, and constitutes the ground for an in-depth systematic stereochemical investigation of a large variety of compounds inside nanotubes and fullerenes.

Conflicts of Interest: The authors declare no conflict of interest

Abbreviations

SWCNTs	single-walled carbon nanotubes
PES	potential energy surface
TS	transition state
DFT	density functional theory
HF	Hartree–Fock
PBE	Perdew–Burke–Ernzerhof
O	Mulliken bond order
HOMO	high occupied molecular orbital
LUMO	low unoccupied molecular orbital
C	conformation of chair form
Tw	conformation of twist form

References

1. Iijima, S. Helical microtubules of graphitic carbon. *Nature* **1991**, *354*, 56–58. [CrossRef]
2. Iijima, S.; Ichihashi, T. Single-shell carbon nanotubes of 1-nm diameter. *Nature* **1993**, *363*, 603–605. [CrossRef]
3. Kroto, H.W.; Heath, J.R.; Obrien, S.C.; Curl, R.F.; Smalley, R.E. C_{60}: Buckminsterfullerene. *Nature* **1985**, *318*, 162–163. [CrossRef]
4. Zhang, R.; Zhang, Y.; Wei, F. Synthesis and Properties of Ultralong Carbon Nanotubes. In *Nanotube Superfiber Materials*; Elsevier: Amsterdam, The Netherlands, 2013; Chapter 4; pp. 87–136. [CrossRef]
5. Nanot, S.; Thompson, N.A.; Kim, J.-H.; Wang, X.; Rice, W.D.; Hároz, E.H.; Ganesan, Y.; Pint, C.L.; Kono, J. Single-Walled Carbon Nanotubes. In *Springer Handbook of Nanomaterials*; Springer Handbooks; Springer: Berlin/Heidelberg, Germany, 2013; pp. 105–146.
6. Tanaka, K.; Iijima, S. Carbon Nanotubes and Graphene, 2nd ed.Elsevier: Amsterdam, The Netherlands, 2014; 458p.
7. Nasrollahzadeh, M.; Issaabadi, Z.; Sajjadi, M.; Sajadi, S.M.; Atarod, M. Types of nanostructures. *Interface Sci. Technol.* **2019**, *28*, 29–80. [CrossRef]
8. Nimibofa, A.; Newton, E.A.; Cyprain, A.Y.; Donbebe, W. Fullerenes: Synthesis and applications. *J. Mater. Sci. Res.* **2018**, *7*, 22–36. [CrossRef]
9. Manzetti, S.; Gabriel, J.-C.P. Methods for dispersing carbon nanotubes for nanotechnology applications: Liquid nanocrystals, suspensions, polyelectrolytes, colloids, and organization control. *Int. Nano Lett.* **2019**, *9*, 31–49. [CrossRef]
10. Takakura, A.; Beppu, K.; Nishihara, T.; Fukui, A.; Kozeki, T.; Namazu, T.; Miyauchi, Y.; Itami, K. Strength of carbon nanotubes depends on their chemical structures. *Nat. Commun.* **2019**, *10*, 3040. [CrossRef]
11. Abdalla, S.; Al-Marzouki, F.; Al-Ghamdi, A.A.; Abdel-Daiem, A. Different technical applications of carbon nanotubes. *Nanoscale Res. Lett.* **2015**, *10*, 358. [CrossRef]
12. Venkataraman, A.; Amadi, E.V.; Chen, Y.; Papadopoulos, C. Carbon nanotube assembly and integration for applications. *Nanoscale Res. Lett.* **2019**, *14*, 220. [CrossRef]
13. Koo, J.H.; Song, J.-K.; Kim, D.-H. Solution-processed thin films of semiconducting carbon nanotubes and their application to soft electronics. *Nanotechnology* **2019**, *30*, 132001. [CrossRef]
14. Akiyama, T. Development of fullerene thin-film assemblies and fullerene-diamine adducts towards practical nanocarbon-based electronic materials. *Bull. Chem. Soc. Jpn.* **2019**, *92*, 1181–1199. [CrossRef]
15. He, H.; Pham-Huy, L.A.; Dramou, P.; Xiao, D.; Zuo, P.; Pham-Huy, C. Carbon nanotubes: Applications in pharmacy and medicine. *BioMed Res. Int.* **2013**, *2013*, 578290. [CrossRef] [PubMed]
16. Sireesha, M.; Babu, V.J.; Kiran, A.S.K.; Ramakrishna, S. A review on carbon nanotubes in biosensor devices and their applications in medicine. *Nanocomposites* **2018**, *4*, 36–57. [CrossRef]
17. Yang, M.; Zhang, M. Biodegradation of carbon nanotubes by macrophages. *Front. Mater.* **2019**, *6*, 225–239. [CrossRef]

18. Castro, E.; Hernandez, G.A.; Zalava, G.; Echegoyen, L. Fullerenes in biology and medicine. *J. Mater. Chem. B* **2017**, *5*, 6523–6535. [CrossRef] [PubMed]

19. Panwar, N.; Soehartono, A.M.; Chan, K.K.; Zeng, S.; Xu, G.; Qu, J.; Coquet, P.; Yong, K.-T.; Chen, X. Nanocarbons for biology and medicine: Sensing, imaging, and drug delivery. *Chem. Rev.* **2019**, *119*, 9559–9656. [CrossRef]

20. Khamitova, K.K.; Kayupov, B.A.; Yegemova, S.S.; Gabdullin, M.T.; Abdullin, K.A.; Ismailov, D.V.; Kerimbekov, D.C. The use of fullerenes as a biologically active molecule. *Int. J. Nanotechnol.* **2019**, *16*, 100–108. [CrossRef]

21. Özkan, E.; Bilge, M.; Bilge, D.; Alver, Ö.; Parlak, C.; Şenyel, M.; Ramasami, P. Sensor application of doped C$_{60}$ fullerenes in detection of 1-(3-trifluoromethylphenyl)piperazine as an alternative to ecstasy. *Main Group Metal. Chem.* **2019**, *42*, 23–27. [CrossRef]

22. Bourassa, D.J.; Kerna, N.A. Pristine. Nanocarbonbased fullerene-like material. Toxicity and biocompatibility (Part 2 in the series: Will Nanocarbon Onion-Like Fullerenes Play a Decisive Role in the Future of Molecular Medicine?). *Determ. Nanomed. Nanotechnol.* **2019**, *1*, DNN.000504.2019.

23. Rahmati, M.; Mozafari, M. Biological response to carbon-family nanomaterials: Interactions at the nano-bio interface. *Front. Bioeng. Biotechnol.* **2019**, *7*, 4. [CrossRef]

24. Yasuno, T.; Ohe, T.; Ikeda, H.; Takahashi, K.; Nakamura, S.; Mashino, T. Synthesis and antitumor activity of novel pyridinium fullerene derivatives. *Int. J. Nanomed.* **2019**, *14*, 6325–6327. [CrossRef] [PubMed]

25. Rodríguez, C.; Leiva, E. Enhanced heavy metal removal from acid mine drainage wastewater using double-oxidized multiwalled carbon nanotubes. *Molecules* **2019**, *25*, 111. [CrossRef] [PubMed]

26. Heath, J.R.; O'Brien, S.C.; Zhang, Q.; Liu, Y.; Curi, R.F.; Kroto, H.W.; Tittel, F.K.; Smalley, R.E. Lanthanum complexes of spheroidal carbon shells. *J. Am. Chem. Soc.* **1985**, *107*, 7779–7780. [CrossRef]

27. Khlobystov, A.N.; Britz, D.A.; Briggs, G.A.D. Molecules in carbon nanotubes. *Acc. Chem. Res.* **2005**, *38*, 901–909. [CrossRef]

28. Tasis, D.; Tagmatarchis, N.; Bianco, A.; Prato, M. Chemistry of carbon nanotubes. *Chem. Rev.* **2006**, *106*, 1105–1136. [CrossRef]

29. Britz, D.A.; Khlobystov, A.N. Noncovalent interactions of molecules with single walled carbon nanotubes. *Chem. Soc. Rev.* **2006**, *35*, 637–659. [CrossRef]

30. Zambrano, H.A.; Walther, J.H.; Koumoutsakos, P.; Sbalzarini, I.F. Thermophoretic motion of water nanodroplets confined inside carbon nanotubes. *Nano Lett.* **2009**, *9*, 66–71. [CrossRef]

31. Liu, X.; Pan, X.; Shen, W.; Ren, P.; Han, X.; Bao, X. NMR study of preferential endohedral adsorption of methanol in multiwalled carbon nanotubes. *J. Phys. Chem. C* **2012**, *116*, 7803–7809. [CrossRef]

32. Sozykin, S.A.; Beskachko, V.P. Structure of endohedral complexes of carbon nanotubes encapsulated with lithium and sodium. *Mol. Phys.* **2013**, *111*, 930–938. [CrossRef]

33. Munusamy, E.; Wheeler, S.E. Endohedral and exohedral complexes of substituted benzenes with carbon nanotubes and graphene. *J. Chem. Phys.* **2013**, *139*, 094703. [CrossRef] [PubMed]

34. Popov, A.A.; Yang, S.; Dunsch, L. Endohedral fullerenes. *Chem. Rev.* **2013**, *113*, 5989–6113. [CrossRef] [PubMed]

35. Manzetti, S. Molecular and crystal assembly inside the carbon nanotube: Encapsulation and manufacturing approaches. *Adv. Manuf.* **2013**, *1*, 198–210. [CrossRef]

36. Tishchenko, O.; Truhlar, D.G. Atom-cage charge transfer in endohedral metallofullerenes: Trapping atoms within a sphere-like ridge of avoided crossings. *J. Phys. Chem. Lett.* **2013**, *4*, 422–425. [CrossRef]

37. Cerón, M.R.; Li, F.-F.; Echegoyen, L.A. Endohedral fullerenes: The importance of electronic, size and shape complementarity between the carbon cages and the corresponding encapsulated clusters. *J. Phys. Org. Chem.* **2014**, *27*, 258–264. [CrossRef]

38. Min, K.; Farimani, A.B.; Aluru, N.R. Mechanically modulated electronic properties of water-filled fullerenes. *MRS Commun.* **2015**, *5*, 305–310. [CrossRef]

39. Umran, N.M.; Kumar, R. Effect on encapsulation (Au and Tl) molecule in fullerene (C$_{60}$) on electronic and magnetic properties. *Quant. Matter* **2015**, *4*, 492–496. [CrossRef]

40. Dargouthi, S.; Boughdiri, S.; Tangour, B. Stabilizing of the transitory species (TiO$_2$)$_2$ by encapsulation into carbon nanotubes. *Acta Chim. Slov.* **2015**, *62*, 445–451. [CrossRef]

41. Nikolaenko, T.Yu.; Kryachko, E.S. Formation of dimers of light noble atoms under encapsulation within fullerene's voids. *Nanoscale Res. Lett.* **2015**, *10*, 185. [CrossRef]

42. Junghans, K.; Rosenkranz, M.; Popov, A.A. $Sc_3CH@C_{80}$: Selective ^{13}C enrichment of the central carbon atom. *Chem. Commun.* **2016**, *52*, 6561–6564. [CrossRef]

43. McSweeney, R.L.; Chamberlain, T.W.; Baldoni, M.; Lebedeva, M.A.; Davies, E.S.; Besley, E.; Khlobystov, A.N. Direct measurement of electron transfer in nanoscale host–guest systems: Metallocenes in carbon nanotubes. *Chem. Eur. J. A* **2016**, *22*, 13540–13549. [CrossRef]

44. Popov, A.A. Synthesis, and molecular structures of endohedral fullerenes. In *Endohedral Fullerenes: Electron Transfer and Spin*; Springer International Publishing AG: Cham, Switzerland, 2017; pp. 1–34. [CrossRef]

45. Kalugina, Y.N.; Roy, P.-N. Potential energy and dipole moment surfaces for $HF@C_{60}$: Prediction of spectral and electric response properties. *J. Chem. Phys.* **2017**, *147*, 244303. [CrossRef]

46. Zhang, R.; Murata, M.; Wakamiya, A.; Shimoaka, T.; Hasegawa, T.; Murata, Y. Isolation of the simplest hydrated acid. *Sci. Adv.* **2017**, *3*, e1602833. [CrossRef]

47. Jin, P.; Yang, L.; Liu, C. Computational prediction of the endohedral metalloborofullerenes $Ti_n@B_{40}$ (n=1, 2). *Theor. Chem. Acc.* **2017**, *136*, 56. [CrossRef]

48. Calatayud, D.G.; Ge, H.; Kuganathan, N.; Mirabello, V.; Jacobs, R.M.J.; Rees, N.H.; Stoppiello, C.T.; Khlobystov, A.N.; Tyrrell, R.M.; Da Como, E.; et al. Encapsulation of cadmium selenide nanocrystals in biocompatible nanotubes: DFT calculations, X-ray diffraction investigations, and confocal fluorescence imaging. *Chem. Open* **2018**, *7*, 144–158. [CrossRef]

49. Poudel, Y.R.; Wenzhi Li, W. Synthesis, properties, and applications of carbon nanotubes filled with foreign materials: A review. *Mater. Today Phys.* **2018**, *7*, 7–34. [CrossRef]

50. Krylov, D.S.; Liu, F.; Brandenburg, A.; Spree, L.; Bon, V.; Kaskel, S.; Wolter, A.U.B.; Büchner, B.; Avdoshenko, S.M.; Popov, A.A. Magnetization relaxation in the single-ion magnet $DySc_2N@C_{80}$: Quantum tunneling, magnetic dilution, and unconventional temperature dependence. *Phys. Chem. Chem. Phys.* **2018**, *20*, 11656–11672. [CrossRef]

51. Mikhailov, G.P. Thermochemistry of complex formation of endofullerene $Li^+@C_{60}$ with the triflate ion. *Russ. J. Gen. Chem.* **2018**, *88*, 2335–2338. [CrossRef]

52. Stasyuk, A.J.; Solà, M.; Voityuk, A.A. Reliable charge assessment on encapsulated fragment for endohedral systems. *Sci. Rep.* **2018**, *8*, 2882. [CrossRef]

53. Xi, C.; Yang, L.; Liu, C.; You, P.; Li, L.; Jin, P. Lanthanide metals in the boron cages: Computational prediction of $M@B_n$ (M = Eu, Gd; n = 38, 40). *Int. J. Quant. Chem.* **2018**, *118*, e25576. [CrossRef]

54. De Munari, S.; Sandoval, S.; Pach, E.; Ballesteros, B.; Tobias, G.; Daniel, C.; Anthony, D.C.; Davis, B.G. *In vivo* behaviour of glyco-NaI@SWCNT 'nanobottles'. *Inorg. Chim. Acta* **2019**, *495*, 118933. [CrossRef]

55. Kuganathan, N.; Chroneos, A. Encapsulation of cadmium telluride nanocrystals within single walled carbon nanotubes. *Inorg. Chim. Acta* **2019**, *488*, 246–254. [CrossRef]

56. Fujii, S.; Cho, H.; Hashikawa, Y.; Nishino, T.; Murata, Y.; Kiguchi, M. Tuneable single-molecule electronic conductance of C_{60} by encapsulation. *Phys. Chem. Chem. Phys.* **2019**, *21*, 12606–12610. [CrossRef]

57. Yang, W.; Velkos, G.; Liu, F.; Sudarkova, S.M.; Wang, Y.; Zhuang, J.; Zhang, H.; Li, X.; Zhang, X.; Büchner, B.; et al. Single molecule magnetism with strong magnetic anisotropy and enhanced Dy···Dy coupling in three isomers of Dy-oxide clusterfullerene $Dy_2O@C_{82}$. *Adv. Sci.* **2019**, *6*, 1901352. [CrossRef]

58. Jin, P.; Li, Y.; Magagula, S.; Chen, Z. Exohedral functionalization of endohedral metallofullerenes: Interplay between inside and outside. *Coord. Chem. Rev.* **2019**, *388*, 406–439. [CrossRef]

59. Ye, L.; Liao, M.; Sun, H.; Yang, Y.; Tang, C.; Zhao, Y.; Wang, L.; Xu, Y.; Zhang, L.; Wang, B.; et al. Stabilizing lithium into cross-stacked nanotube sheets with an ultra-high specific capacity for lithium oxygen batteries. *Angew. Chem. Int. Ed.* **2019**, *58*, 2437–2442. [CrossRef]

60. Zhao, Y.-X.; Li, M.-Y.; Xiong, Y.-M.; Rahmani, S.; Yuan, K.; Zhao, R.-S.; Ehara, M.; Nagase, S.; Zhao, X. Pivotal role of nonmetal atoms in the stabilities, geometries, electronic structures, and isoelectronic chemistry of $Sc_3X@C_{80}$ (X = C, N, and O). *J. Comput. Chem.* **2019**, *40*, 2730–2738. [CrossRef]

61. Bloodworth, S.; Sitinova, G.; Alom, S.; Vidal, S.; Bacanu, G.R.; Elliott, S.J.; Light, M.E.; Herniman, J.M.; Langley, G.J.; Levitt, M.H.; et al. First synthesis and characterization of $CH_4@C_{60}$. *Angew. Chem. Int. Ed.* **2019**, *58*, 5038–5043. [CrossRef]

62. Sheikhi, M.; Shahab, S.; Alnajjar, R.; Ahmadianarog, M. Theoretical model for surface forces between cytosine and CNT(6,6-6) nanotube: Geometry optimization, molecular structure, intermolecular hydrogen bond, spectroscopic (NMR, UV/Vis, excited state), FMO, MEP, and HOMO–LUMO investigation. *Russ. J. Phys. Chem. A* **2019**, *93*, 2429–2443. [CrossRef]

63. Jiang, Y.; Wang, C. Endohedral and exohedral complexes of 1-benzene with carbon nanotubes and high-density assembly of multiple benzenes inside of a carbon nanotube. *Int. J. Quant. Chem.* **2019**, *119*, e25936. [CrossRef]

64. Wang, J.T.-W.; Klippstein, R.; Martincic, M.; Pach, E.; Feldman, R.; Šefl, M.; Michel, Y.; Asker, D.; Sosabowski, J.K.; Kalbac, M.; et al. Neutron activated ^{153}Sm sealed in carbon nanocapsules for *in vivo* imaging and tumor radiotherapy. *ACS Nano* **2020**, *14*, 129–141. [CrossRef]

65. Wei, T.; Martin, O.; Chen, M.; Yang, S.; Hauke, F.; Hirsch, A. Covalent inter-carbon-allotrope architectures consisting of the endohedral fullerene $Sc_3N@C_{80}$ and single-walled carbon nanotubes. *Angew. Chem. Int. Ed.* **2019**, *58*, 8058–8062. [CrossRef]

66. Dappe, Y.J. Encapsulation of organic molecules in carbon nanotubes: Role of the van der Waals interactions. *J. Phys. D Appl. Phys.* **2014**, *47*, 083001. [CrossRef]

67. Gtari, W.F.; Tangour, B. Interaction of HF, HBr, HCl and HI molecules with carbon nanotubes. *Acta Chim. Slov.* **2018**, *65*, 289–295. [CrossRef]

68. Halls, M.D.; Schlegel, H.B. Chemistry inside carbon nanotubes: the Menshutkin S_N2 reaction. *J. Phys. Chem. B* **2002**, *106*, 1921–1925. [CrossRef]

69. Halls, M.D.; Raghavachari, K. Carbon nanotube inner phase chemistry: The Cl^- exchange S_N2 reaction. *Nano Lett.* **2005**, *5*, 1861–1866. [CrossRef]

70. Botos, A.; Biskupek, J.; Chamberlain, T.W.; Rance, G.A.; Stoppiello, C.T.; Sloan, J.; Liu, Z.; Suenaga, K.; Kaiser, U.; Khlobystov, A.N. Carbon nanotubes as electrically active nanoreactors for multi-step inorganic synthesis: Sequential transformations of molecules to nanoclusters and nanoclusters to nanoribbons. *J. Am. Chem. Soc.* **2016**, *138*, 8175–8183. [CrossRef]

71. Miners, S.A.; Rance, G.A.; Khlobystov, A.N. Chemical reactions confined within carbon nanotubes. *Chem. Soc. Rev.* **2016**, *45*, 4727–4746. [CrossRef]

72. Astle, M.A.; Rance, G.A.; Fay, M.W.; Notman, S.; Sambrook, M.R.; Khlobystov, A.N. Synthesis of hydroxylated group IV metal oxides inside hollow graphitised carbon nanofibers: Nano-sponges and nanoreactors for enhanced decontamination of organophosphates. *J. Mater. Chem. A* **2018**, *6*, 20444–20453. [CrossRef]

73. Astle, M.A.; Rance, G.A.; Loughlin, H.J.; Peters, T.D.; Khlobystov, A.N. Molybdenum dioxide in carbon nanoreactors as a catalytic nanosponge for the efficient desulfurization of liquid fuels. *Adv. Funct. Mater.* **2019**, *29*, 1808092. [CrossRef]

74. Fay, M.W.; Baldoni, M.; Besley, E.; Khlobystov, A.N.; Rance, G.A. Steric and electronic control of 1,3-dipolar cycloaddition reactions in carbon nanotube nanoreactors. *J. Phys. Chem. C* **2019**, *123*, 6294–6302. [CrossRef]

75. Agasti, N.; Astle, M.A.; Rance, G.A.; Fernandes, J.A.; Dupont, J.; Khlobystov, A.N. Cerium oxide nanoparticles inside carbon nanoreactors for selective allylic oxidation of cyclohexene. *Nano Lett.* **2020**, *20*, 1161–1171. [CrossRef]

76. Rance, G.A.; Miners, S.A.; Chamberlain, T.W.; Khlobystov, A.N. The effect of carbon nanotubes on chiral chemical reactions. *Chem. Phys. Lett.* **2013**, *557*, 10–14. [CrossRef]

77. Reichardt, C. *Solvents and Solvent Effects in Organic Chemistry*; WILEY-VCH Verlag GmbH & Co. KGaA: Weinheim, Germany, 2003; pp. 5–91.

78. Mennucci, B. Solvation Models for Molecular Properties: Continuum versus Discrete Approaches. In *Solvation Effects on Molecules and Biomolecules. Computational Methods and Applications*; Springer Science & Business Media: Berlin/Heidelberg, Geramny, 2010; pp. 1–21.

79. Eilmes, A. Solvatochromic probe in molecular solvents: Implicit versus explicit solvent model. *Theor. Chem. Acc.* **2014**, *133*, 1538. [CrossRef]

80. Gaalswyk, K.; Rowley, C.N. An explicit-solvent conformation search method using open software. *Peer J.* **2016**, *4*, e2088. [CrossRef]

81. Zhang, J.; Zhang, H.; Wu, T.; Wang, Q.; Spoel, D. Comparison of implicit and explicit solvent models for the calculation of solvation free energy in organic solvents. *J. Chem. Theory Comput.* **2017**, *13*, 1034–1043. [CrossRef]

82. Turner, M.A.P.; Turner, R.J.; Horbury, M.D.; Hine, N.D.M.; Stavros, V.G. Examining solvent effects on the ultrafast dynamics of catechol. *J. Chem. Phys.* **2019**, *151*, 084305. [CrossRef]

83. Varghese, J.J.; Mushrif, S.H. Origins of complex solvent effects on chemical reactivity and computational tools to investigate them: A review. *React. Chem. Eng.* **2019**, *4*, 165–206. [CrossRef]

84. Sattasathuchana, T.; Xu, P.; Gordon, M.S. An Accurate quantum-based approach to explicit solvent effects: Interfacing the general effective fragment potential method with *ab initio* electronic structure theory. *J. Phys. Chem. A* **2019**, *123*, 8460–8475. [CrossRef]

85. Avramov, P.V.; Kudin, K.N.; Scuseria, G.E. Single wall carbon nanotubes density of states: Comparison of experiment and theory. *Chem. Phys. Lett.* **2003**, *370*, 597–601. [CrossRef]

86. Koner, A.; Kumar, C.; Sathyamurthy, N. Heat capacity of endohedral fullerenes $Rg@C_{60}$ (Rg = He, Ne, Ar and Kr). *Mol. Phys.* **2018**, *116*, 2728–2735. [CrossRef]

87. Laikov, D.N.; Ustynyuk, Y.A. PRIRODA-04: A quantum-chemical program suite. New possibilities in the study of molecular systems with the application of parallel computing. *Russ. Chem. Bull.* **2005**, *54*, 820–826. [CrossRef]

88. Sabirov, D.S. Anisotropy of polarizability of fullerene higher adducts for assessing the efficiency of their use in organic solar cells. *J. Phys. Chem. C* **2013**, *117*, 9148–9153. [CrossRef]

89. Sabirov, D.S. From endohedral complexes to endohedral fullerene covalent derivatives: A density functional theory prognosis of chemical transformation of water endofullerene $H_2O@C_{60}$ upon its compression. *J. Phys. Chem. C* **2013**, *117*, 1178–1182. [CrossRef]

90. Pankratyev, E.Y.; Tukhbatullina, A.A.; Sabirov, D.S. Dipole polarizability, structure, and stability of [2+2]-linked fullerene nanostructures $(C_{60})_n$ ($n \leq 7$). *Physica E* **2017**, *86*, 237–242. [CrossRef]

91. Pankratyev, E.Y.; Khatymov, R.V.; Sabirov, D.S.; Yuldashev, A.V. On the upper bound of the thermodynamic stability of fullerenes from small to giant. *Physica E* **2018**, *101*, 265–272. [CrossRef]

92. Laikov, D.N. Fast evaluation of density functional exchange-correlation terms using the expansion of the electron density in auxiliary basis sets. *Chem. Phys. Lett.* **1997**, *281*, 151–156. [CrossRef]

93. Ramachandran, C.N.; Fazio, D.D.; Sathyamurthy, N.; Aquilanti, V. Guest species trapped inside carbon nanotubes. *Chem. Phys. Lett.* **2009**, *473*, 146–150. [CrossRef]

94. *Internal Rotation in Molecules*; Orville-Thomas, W.J. (Ed.) Wiley-Interscience: London, UK; New York, NY, USA, 1974; p. 606.

95. Pophristic, V.; Goodman, L. Exchange repulsion increases internal rotation floppiness. *J. Chem. Phys.* **2001**, *115*, 5132–5136. [CrossRef]

96. Kundu, T.; Pradhan, B.; Singh, B.P. Origin of methyl torsional potential barrier—An overview. *J. Chem. Sci.* **2002**, *114*, 623–638. [CrossRef]

97. Bickelhaupt, F.M.; Baerends, E.J. The case for steric repulsion causing the staggered conformation of ethane. *Angew. Chem. Int. Ed.* **2003**, *42*, 4183–4188. [CrossRef]

98. Rico, J.F.; López, R.; Ema, I.; Ramirez, G. Density and binding forces: Rotational barrier of ethane. *J. Chem. Phys.* **2003**, *119*, 12251–12256. [CrossRef]

99. Sadlej-Sosnowska, N. Energy barriers to internal rotation: Hyperconjugation and electrostatic description. *J. Phys. Chem. A* **2003**, *107*, 8671–8676. [CrossRef]

100. Song, L.; Lin, Y.; Zhang, Q.; Mo, Y. Steric strain versus hyperconjugative stabilization in ethane congeners. *J. Phys. Chem. A* **2005**, *109*, 2310–2316. [CrossRef]

101. Liu, S.B. Steric effect: A quantitative description from density functional theory. *J. Chem. Phys.* **2007**, *126*, 244103. [CrossRef]

102. Mo, Y.; Gao, J. Theoretical analysis of the rotational barrier of ethane. *Acc. Chem. Res.* **2007**, *40*, 113–119. [CrossRef]

103. Liu, S.B.; Govind, N. Toward understanding the nature of internal rotation barriers with a new energy partition scheme: Ethane and n-butane. *J. Phys. Chem. A* **2008**, *112*, 6690–6699. [CrossRef]

104. Liu, S.B.; Govind, N.; Pedersen, L.G. Exploring the origin of the internal rotational barrier for molecules with one rotatable dihedral angle. *J. Chem. Phys.* **2008**, *129*, 094104. [CrossRef]

105. Mo, Y. Rotational barriers in alkanes. *WIREs Comput. Mol. Sci.* **2011**, *1*, 164–171. [CrossRef]

106. Esquivel, R.O.; Liu, S.B.; Angulo, J.C.; Dehesa, J.S.; Antolin, J.; Molina-Espiritu, M. Fisher information and steric effect: Study of the internal rotation barrier of ethane. *J. Phys. Chem. A* **2011**, *115*, 4406–4415. [CrossRef]

107. Quijano-Quiñones, R.F.; Quesadas-Rojas, M.; Cuevas, G.; Mena-Rejón, G.J. The Rotational barrier in ethane: A molecular orbital study. *Molecules* **2012**, *17*, 4661–4671. [CrossRef]

108. Liu, S.B. Origin and nature of bond rotation barriers: A unified view. *J. Phys. Chem. A* **2013**, *117*, 962–965. [CrossRef]

109. Liu, S.B.; Schauer, C.K. Origin of molecular conformational stability: Perspectives from molecular orbital interactions and density functional reactivity theory. *J. Chem. Phys.* **2015**, *142*, 054107. [CrossRef]

110. Baranac-Stojanović, M. Theoretical analysis of the rotational barrier in ethane: Cause and consequences. *Struct. Chem.* **2015**, *26*, 989–996. [CrossRef]

111. Priebe, A.; Pucci, A.; Akemann, W.; Grabhorn, H.; Otto, A. Staggered ethane changes to eclipsed conformation upon adsorption. *J. Raman Spect.* **2006**, *37*, 1398–1402. [CrossRef]

112. Wanjari, P.P.; Sangwai, A.V.; Ashbaugh, H.S. Confinement induced conformational changes in *n*-alkanes sequestered within a narrow carbon nanotube. *Phys. Chem. Chem. Phys.* **2012**, *14*, 2702–2709. [CrossRef]

113. Velpuri, S.V.V.; Gade, H.M.; Wanjari, P.P. Encapsulation driven conformational changes in *n*-alkanes inside a hydrogen-bonded supramolecular cavitand assembly. *Chem. Phys.* **2019**, *521*, 100–107. [CrossRef]

114. Gade, H.M.; Velpuri, S.V.V.; Wanjari, P.P. Conformational rearrangements in *n*-alkanes encapsulated within capsular self-assembly of capped carbon nanotubes. *Chem. Phys.* **2019**, *517*, 198–207. [CrossRef]

115. Bates, S.P.; van Well, W.J.M.; van Santen, R.A.; Smit, B. Location and conformation of n-alkanes in zeolites: An analysis of configurational-bias Monte Carlo calculations. *J. Phys. Chem.* **1996**, *100*, 17573–17581. [CrossRef]

116. Gorgoll, R.M.; Yücelen, E.; Kumamoto, A.; Shibata, N.; Harano, K.; Nakamura, E. Electron microscopic observation of selective excitation of conformational change of a single organic molecule. *J. Am. Chem. Soc.* **2015**, *137*, 3474–3477. [CrossRef]

117. Harano, K.; Takenaga, S.; Okada, S.; Niimi, Y.; Yoshikai, N.; Isobe, H.; Suenaga, K.; Kataura, H.; Koshino, M.; Nakamura, E. Conformational analysis of single perfluoroalkyl chains by single-molecule real-time transmission electron microscopic imaging. *J. Am. Chem. Soc.* **2014**, *136*, 466–473. [CrossRef]

118. Zhang, X.; Wang, W. Adsorption of linear ethane molecules in single walled carbon nanotube arrays by molecular simulation. *Phys. Chem. Chem. Phys.* **2002**, *4*, 3048–3054. [CrossRef]

119. Jakobtorweihen, S.; Keil, F.G. Adsorption of alkanes, alkenes and their mixtures in single-walled carbon nanotubes and bundles. *Mol. Simul.* **2009**, *35*, 90–99. [CrossRef]

120. Cruz, F.J.A.L.; Müller, E.A. Behavior of ethylene and ethane within single-walled carbon nanotubes. 1: Adsorption and equilibrium properties. *Adsorption* **2009**, *15*, 1–12. [CrossRef]

121. Cruz, F.J.A.L.; Müller, E.A. Behavior of ethylene and ethane within single-walled carbon nanotubes, 2: Dynamical properties. *Adsorption* **2009**, *15*, 13–22. [CrossRef]

122. Albesa, A.G.; Matías Rafti, M.; Rawat, D.S.; Vicente, J.L.; Migone, A.D. Ethane/ethylene adsorption on carbon nanotubes: Temperature and size effects on separation capacity. *Langmuir* **2012**, *28*, 1824–1832. [CrossRef]

123. Tian, X.; Wang, Z.; Yang, Z.; Xiu, P.; Zhou, B. Adsorptive separation of ethylene/ethane mixtures using carbon nanotubes: A molecular dynamics study. *J. Phys. D Appl. Phys.* **2013**, *46*, 395302. [CrossRef]

124. Boudry, J. van der Waals interactions and decrease of the rotational barrier of methyl-sized rotators: A theoretical study. *J. Am. Chem. Soc.* **2006**, *128*, 11088–11093. [CrossRef]

125. Kuznetsov, V.V. Theoretical evaluation of conformational preference of ethane molecule encapsulated in a nanotube. *Russ. J. Org. Chem.* **2013**, *49*, 313–314. [CrossRef]

126. Kuznetsov, V.V. Conformational behavior of ethane molecule encapsulated in a nanotube. *Russ. J. Org. Chem.* **2013**, *49*, 1231–1235. [CrossRef]

127. Kuznetsov, V.V. Influence of the nanotube type on the conformational behavior of encapsulated ethane molecule. *Russ. J. Gen. Chem.* **2013**, *83*, 2334–2336. [CrossRef]

128. Kuznetsov, V.V. Conformational properties of ethane and its analogs in nanotubes. *Russ. J. Gen. Chem.* **2019**, *89*, 1271–1278. [CrossRef]

129. Wang, P.; Zhang, C. Doped ways of boron and nitrogen doped carbon nanotubes: A theoretical investigation. *J. Mol. Struct. (THEOCHEM)* **2010**, *955*, 84–90. [CrossRef]

130. Rimola, A.; Sodure, M. Gas-phase and microsolvated glycine interacting with boron nitride nanotubes. A B3LYP-D2* periodic study. *Inorganics* **2014**, *2*, 334–350. [CrossRef]

131. Tenne, R.; Enyashkin, A.N. Inorganic fullerene-like nanoparticles and inorganic nanotubes. *Inorganics* **2014**, *2*, 649–651. [CrossRef]

132. Kuznetsov, V.V. Theoretical evaluation of conformational preference of the propane molecule in nanotubes. *Russ. J. Gen. Chem.* **2013**, *83*, 1165–1166. [CrossRef]

133. Bartell, L.S.; Boates, T.L. Structures of the strained molecules hexamethylethane and 1,1,2,2-tetramethylethane by gas-phase electron diffraction. *J. Mol. Struct.* **1976**, *32*, 379–392. [CrossRef]

134. Kuznetsov, V.V. Theoretical evaluation of conformational preference of the 2,2,3,3-tetramethylbutane molecule in nanotubes. *Russ. J. Gen. Chem.* **2013**, *83*, 1455–1456. [CrossRef]

135. Hembree, W.I.; Boudry, J. Three-dimensional mapping of microenvironmental control of methyl rotational barriers. *J. Phys. Chem. B* **2011**, *115*, 8575–8580. [CrossRef]

136. Weiss, S.; Leroi, G.E. Infrared spectra and internal rotation in propane, isobutane and neopentane. *Spectrochim. Acta. A* **1969**, *25*, 1759–1766. [CrossRef]

137. Holm, U.; Kerl, K. Anomalous behaviour of the mean dipole polarizability α of neopentane $C(CH_3)_4$ in the temperature range between 250 K and 360 K. *Z. Naturforsch. A* **1991**, *46*, 983–988. [CrossRef]

138. Kuznetsov, V.V. Conformational preferences of 2,2-dimethylpropane in nanotubes. *Russ. J. Gen. Chem.* **2014**, *84*, 433–438. [CrossRef]

139. Chen, S.S.; Rodgers, A.C.; Chao, J.; Wilhoit, R.C.; Zwolinski, B.J. Ideal gas thermodynamic properties of six fluoroethanes. *J. Phys. Chem. Ref. Data* **1975**, *4*, 441–456. [CrossRef]

140. Kuznetsov, V.V. Conformational analysis of fluoroethane in nanotubes. *Russ. J. Org. Chem.* **2018**, *54*, 644–651. [CrossRef]

141. Brier, P.N.; Higgins, S. Neutron inelastic scattering measurements on 1,1,1-trifluoroethane. *J. Mol. Phys.* **1970**, *19*, 645–657. [CrossRef]

142. Kuznetsov, V.V. Conformational behavior of 1,1,1-trifluoroethane in nanotubes. *Russ. J. Org. Chem.* **2014**, *50*, 1534–1539. [CrossRef]

143. Kuznetsov, V.V. Theoretical evaluation of conformational preference of the hexafluoroethane molecule in nanotubes. *Russ. J. Gen. Chem.* **2013**, *83*, 1623–1625. [CrossRef]

144. Thorne, L.R.; Suenram, R.D.; Lovas, F.J. Microwave spectrum, torsional barrier, and structure of BH_3NH_3. *Chem. Phys.* **1983**, *78*, 167–171. [CrossRef]

145. Parafiniuk, M.; Mitoraj, M.P. On the origin of internal rotation in ammonia borane. *J. Mol. Model.* **2014**, *20*, 2272. [CrossRef]

146. Demirci, U.B. Ammonia borane, a material with exceptional properties for chemical hydrogen storage. *Int. J. Hydrogen Energy* **2017**, *42*, 9978–10013. [CrossRef]

147. Akbayrak, S.; Özkar, S. Ammonia borane as hydrogen storage materials. *Int. J. Hydrogen Energy* **2018**, *43*, 18592–18606. [CrossRef]

148. Li, L.; Yao, X.; Sun, C.; Du, A.; Cheng, L.; Zhu, Z.; Yu, C.; Zou, J.; Smith, S.C.; Wang, P.; et al. Lithium-catalyzed dehydrogenation of ammonia borane within mesoporous carbon framework for chemical hydrogen storage. *Adv. Funct. Mater.* **2009**, *19*, 265–271. [CrossRef]

149. Wahab, M.A.; Zhao, H.; Yao, X.D. Nano-confined ammonia borane for chemical hydrogen storage. *Front. Chem. Sci. Eng.* **2012**, *6*, 27–33. [CrossRef]

150. Zhang, L.; Xia, G.; Ge, Y.; Wang, C.; Guo, Z.; Li, X.; Yu, X. Ammonia borane confined by nitrogen-containing carbon nanotubes: Enhanced dehydrogenation properties originating from synergetic catalysis and nanoconfinement. *J. Mater. Chem. A* **2015**, *3*, 20494–20499. [CrossRef]

151. Kuznetsov, V.V. Ammonia borane in nanotubes: The preference of eclipsed conformation. *Russ. J. Inorg. Chem.* **2018**, *63*, 1069–1075. [CrossRef]

152. Urban, J.; Schireiner, P.R.; Vacec, G.; von RaguéSchleyer, P.; Huang, J.Q.; Leszczynski, J. Molecular structures, vibrational spectra, and rotational barriers of C_2H_6, Si_2H_6, $SiGeH_6$, and Ge_2H_6—experiment and theory in harmony. *Chem. Phys. Lett.* **1997**, *264*, 441–448. [CrossRef]

153. Puzzarini, C. Accurate structure and torsional barrier height of disilane. *Phys. Chem. Chem. Phys.* **2003**, *5*, 26–30. [CrossRef]

154. Pophristic, V.; Goodman, L.; Wu, C.T. Disilane internal rotation. *J. Phys. Chem. A* **2001**, *105*, 7454–7459. [CrossRef]

155. Kuznetsov, V.V. Nanotube effect on conformation of encapsulated disilane molecule. *Russ. J. Gen. Chem.* **2015**, *85*, 1989–1991. [CrossRef]

156. Durig, J.R.; Church, J.S. Vibrational spectra of crystalline disilane and disilane-d_6, barrier to internal rotation and some normal coordinate calculations on H_3SiSiH_3, H_3SiNCO, and H_3SiNCS. *J. Chem. Phys.* **1980**, *73*, 4784–4797. [CrossRef]

157. Dows, D.A.; Hexter, R.M. Infrared spectra of gaseous and solid digermane. *J. Chem. Phys.* **1956**, *24*, 1029–1033. [CrossRef]

158. Isobe, C.; Cho, H.-C.; Crowell, J.E. The photo-induced reaction of digermane with the Si(100)(2 × 1):D surface. *Surf. Sci.* **1993**, *295*, 117–132. [CrossRef]

159. Hart, J.; Hazbun, R.; Eldridge, D.; Hickey, R.; Femando, N.; Adam, T.; Zollner, S.; Kolodzey, J. Tetrasilane and digermane for the ultra-high vacuum chemical vapor deposition of SiGe alloys. *Thin Solid Film* **2016**, *604*, 23–27. [CrossRef]

160. Lin, D.-S.; Huang, K.-H.; Pi, T.-W.; Wu, R.-T. Coverage-dependent thermal reactions of digermane on Si(100)-(2×1). *Phys. Rev. B* **1996**, *54*, 16958–16964. [CrossRef] [PubMed]

161. Hatmann, J.-M.; Aubin, J.; Barnes, J.-P. A benchmark of germane and digermane for the low temperature growth of intrinsic and heavily *in-situ* boron-doped SiGe. *ECS Trans.* **2016**, *75*, 281–294. [CrossRef]

162. Hart, J.; Adam, T.; Kim, Y.; Huang, Y.-Ch.; Reznicer, A.; Hazbun, R.; Gupta, J.; Kolodzey, J. Temperature varying photoconductivity of GeSn alloys grown by chemical vapor deposition with Sn concentrations from 4% to 11%. *J. Appl. Phys.* **2016**, *119*, 093105. [CrossRef]

163. Lu, G.; Crowell, J.E. The adsorption and thermal decomposition of digermane on Ge(111). *J. Chem. Phys.* **1993**, *98*, 3415–3421. [CrossRef]

164. Aubin, J.; Hartmann, J.M.; Buer, M.; Moffatt, S. Very low temperature epitaxy of Ge and Ge rich SiGe alloy with Ge_2H_6 in a reduced pressure—Chemical vapor deposition tool. *J. Cryst. Growth* **2016**, *445*, 65–72. [CrossRef]

165. Kuznetsov, V.V.; Bochkor, S.A. Relative stability of digermane conformers in nanotubes. *Russ. J. Gen. Chem.* **2020**, *90*, 93–98. [CrossRef]

166. Gropen, O.; Johansen, R. Barrier of internal rotation and π-bonding in hydroxyborane, H_2BOH, studied by ab initio calculations. *J. Mol. Struct.* **1975**, *25*, 161–167. [CrossRef]

167. Lanthier, G.F.; Graham, W.A.G. Dimethylboric anhydride: A convenient preparation and full characterization. *Can. J. Chem.* **1969**, *47*, 569–575. [CrossRef]

168. Finocchiaro, P.; Gust, D.; Mislow, K. Conformational dynamics of alkoxydiarylboranes. *J. Am. Chem. Soc.* **1973**, *95*, 7029–7036. [CrossRef]

169. Brown, N.M.D.; Davidson, F.; Wilson, J.W. Dimesitylboryl compounds. VI. ^{13}C Dynamic nuclear magnetic resonance studies. *J. Organometal. Chem.* **1981**, *210*, 1–8. [CrossRef]

170. Stampf, E.J.; Odom, J.D.; Saari, S.V.; Kim, Y.H.; Bergana, M.M.; During, J.R. Dimethylmethoxyborane: Vibrational assignment, conformational stability, ab initio calculations and barriers to internal rotation. *J. Mol. Struct.* **1990**, *239*, 113–137. [CrossRef]

171. Kuznetsov, V.V. Conformation of hydroxyborane encapsulated within nanotubes. *Russ. J. Gen. Chem.* **2014**, *84*, 157–159. [CrossRef]

172. Vincent, M.A.; Schaefer, H.F. Diborane(4) (B_2H_4): The boron hydride analog of ethylene. *J. Am. Chem. Soc.* **1981**, *103*, 5677–5680. [CrossRef]

173. Lein, M.; Szabó, A.; Kovács, A.; Frenking, G. Energy decomposition analysis of the chemical bond in main group and transition metal compound. *Faraday Discuss.* **2003**, *124*, 365–378. [CrossRef]

174. Osorio, E.; Olson, J.K.; Tiznado, W.; Boldyrev, A.I. Analysis of why boron avoids sp^2 hybridization and classical structures in the B_nH_{n+2} series. *Chem. Eur. J.* **2012**, *18*, 9677–9681. [CrossRef]

175. Kuznetsov, V.V. The influence of carbon nanotubes on the relative stability of diborane molecular forms. *Russ. J. Gen. Chem.* **2016**, *86*, 231–240. [CrossRef]

176. Lammertsma, K.; Güner, O.F.; Drewes, R.M.; Reed, A.E.; Schleyer, P.R. Remarkable structures of dialane(4), Al_2H_4. *Inorg. Chem.* **1989**, *28*, 313–317. [CrossRef]

177. Wang, X.; Andrews, L.; Tam, S.; DeRose, M.E.; Fajardo, M.E. Infrared spectra of aluminum hydrides in solid hydrogen: Al_2H_4 and Al_2H_6. *J. Am. Chem. Soc.* **2003**, *125*, 9218–9228. [CrossRef]

178. Lazarev, V.V.; Kuznetsov, V.V. Influence of nanotubes on the relative stability of orthogonal form of dialane. *Russ. J. Gen. Chem.* **2019**, *89*, 1792–1799. [CrossRef]

179. Schlegel, H.B.; Skancke, A. Thermochemistry, energy comparisons, and conformational analysis of hydrazine, triazane, and triaminoammonia. *J. Am. Chem. Soc.* **1993**, *115*, 7465–7471. [CrossRef]

180. Kobychev, V.B.; Vitkovskaya, N.M.; Pavlova, N.V.; Schmidt, E.Yu.; Trofimov, B.A. Theoretical analysis and experimental study of the spatial structure and isomerism of acetone azine and its cyclization to 3,5,5-trimethyl-4,5-dihydro-1*H*-pyrazole. *J. Struct. Chem.* **2004**, *45*, 748–755. [CrossRef]

181. Song, L.; Liu, M.; Wu, W.; Zhang, Q.; Mo, Y. Origins of rotational barriers in hydrogen peroxide and hydrazin. *J. Chem. Theory Comput.* **2005**, *1*, 394–402. [CrossRef] [PubMed]

182. Łodyga, W.; Makarewicz, J. Torsion-wagging tunneling and vibrational states in hydrazine determined from its *ab initio* potential energy surface. *J. Chem. Phys.* **2012**, *136*, 174301. [CrossRef] [PubMed]

183. Kuznetsov, V.V. Hydrazine: Structural features and conformational preference in nanotubes. *Russ. J. Gen. Chem.* **2016**, *86*, 2000–2007. [CrossRef]

184. Lees, R.M.; Mohammadi, M.A. Millimetre wave spectrum of methyl mercaptan. *Can. J. Phys.* **1980**, *58*, 1640–1648. [CrossRef]

185. Kuznetsov, V.V. Conformational behavior of methanol in a nanotube. *Russ. J. Org. Chem.* **2014**, *50*, 765–766. [CrossRef]

186. Tuazon, E.C.; Fateley, W.G. Internal rotation in $(CH_3)_2X$ molecules of C2v symmetry–barrier to internal rotation in dimethyl ether. *J. Chem. Phys.* **1971**, *54*, 4450–4454. [CrossRef]

187. Endres, C.P.; Drouin, B.J.; Pearson, J.C.; Müller, H.S.P.; Lewen, F.; Schlemmer, S.; Giesen, T.F. Dimethyl ether: Laboratory spectra up to 2.1 THz. Torsion-rotational spectra within the vibrational ground state. *Astron. Astrophys.* **2009**, *504*, 635–640. [CrossRef]

188. Kimura, K.; Kubo, M. Structures of dimethyl ether and methyl alcohol. *J. Chem. Phys.* **1959**, *30*, 151–158. [CrossRef]

189. Blukis, U.; Kasai, P.H.; Myers, R.J. Microwave spectra and structure of dimethyl ether. *J. Chem. Phys.* **1963**, *38*, 2753–2760. [CrossRef]

190. Goodman, L.; Pophristic, V. Where does the dimethyl ether internal rotation barrier come from? *Chem. Phys. Lett.* **1996**, *259*, 287–295. [CrossRef]

191. Pophristic, V.; Goodman, L.; Guchhait, N. Role of lone-pairs in internal rotation barriers. *J. Phys. Chem. A* **1997**, *101*, 4290–4297. [CrossRef]

192. Pophristic, V.; Goodman, L. Influence of protonation on internal rotation of dimethyl ether. *J. Phys. Chem. A* **2000**, *104*, 3231–3238. [CrossRef]

193. Jimenez-Fabian; Jalbout, A.F. The origin of the rotational barrier in dimethyl ether and dimethyl sulfide. A theoretical study. *J. Theor. Comput. Chem.* **2007**, *6*, 421–434. [CrossRef]

194. Kuznetsov, V.V. Dimethyl ether in nanotubes: Structural variations and conformational preferences. *Russ. J. Gen. Chem.* **2016**, *86*, 1835–1840. [CrossRef]

195. Kuznetsov, V.V. Fullerene Si_{20}: Influence on the conformational behavior of encapsulated ethane molecule. *Russ. J. Gen. Chem.* **2016**, *86*, 1444–1446. [CrossRef]

196. Kuznetsov, V.V. Theoretical evaluation of conformational preference of the ethane molecule in fullerene C_{60}. *Russ. J. Gen. Chem.* **2013**, *83*, 1163–1164. [CrossRef]

197. Kuznetsov, V.V. Conformational preference of hexafluoroethane molecule encapsulated in fullerenes. *Russ. J. Org. Chem.* **2014**, *50*, 456–457. [CrossRef]

198. Kuznetsov, V.V. The effect of chemical composition of the fullerene on the conformational preference of the encapsulated hexafluoroethane molecule. *Russ. J. Gen. Chem.* **2016**, *86*, 1108–1114. [CrossRef]

199. Kuznetsov, V.V. Conformational preference of the hexachloroethane molecule in fullerene C_{80}. *Russ. J. Gen. Chem.* **2013**, *83*, 1790–1791. [CrossRef]

200. Kuznetsov, V.V. Conformation of 2,2-dimethylpropane encapsulated in fullerenes. *Russ. J. Org. Chem.* **2014**, *50*, 921–922. [CrossRef]

201. Shakirova, E.I.; Kuznetsov, V.V. Effect of chemical composition of fullerenes on the structure and internal rotation barrier of encapsulated ammonia borane molecule. *Russ. J. Gen. Chem.* **2019**, *89*, 2229–2234. [CrossRef]

202. Kuznetsov, V.V.; Bochkor, S.A. The influence of chemical composition of fullerenes on the structural features and conformational preference of encapsulated disilane molecule. *Russ. J. Inorg. Chem.* **2018**, *63*, 917–922. [CrossRef]

203. Kuznetsov, V.V. Conformational behavior of methanethiol in fullerenes. *Russ. J. Org. Chem.* **2014**, *50*, 1073–1074. [CrossRef]

204. Kuznetsov, V.V. Cyclohexane in nanotubes: Direct chair–chair interconversion. *Russ. J. Gen. Chem.* **2017**, *87*, 2558–2562. [CrossRef]

205. Ram, V.J.; Sethi, A.; Nath, M.; Pratar, R. *The Chemistry of Heterocycles. Chemistry of Six- to Eight-Membered N, O, S, P and Se Heterocycles*; Elsevier: Amsterdam, The Netherlands, 2019; pp. 340–392. [CrossRef]

206. Franchini, S.; Sorbi, C.; Linciano, P.; Camevale, G.; Tait, A.; Ronsisvalle, S.; Buccioni, M.; Del Bello, F.; Cilia, A.; Pironal, L.; et al. **1**,3-Dioxane as a scaffold for potent and selective 5-HT$_{1A}$R agonist with *in-vivo* anxiolytic, anti-depressant and anti-nociceptive activity. *Eur. J. Med. Chem.* **2019**, *176*, 310–325. [CrossRef]

207. Janssens, J.; Risseeuw, M.D.P.; Eycken, J.V.; Calenbergh, S.V. Regioselective ring opening of 1,3-dioxane-type acetals in carbohydrates. *Eur. J. Org. Chem.* **2018**, *2018*, 6405–6431. [CrossRef]

208. Cooksey, J.; Gunn, A.; Philip, J.; Kocienski, P.J.; Kuhl, A.; Uppal, S.; Christopher, J.A.; Bell, R. The nucleophilic addition of α-metallated 1,3-dioxanes to planar chiral cationic η^3-allylmolybdenum complexes. Synthesis of (2*E*,5*S*,6*R*,7*E*)-6-methyl-8-phenylocta-2,7-dienoic acid methyl ester, a key component of the cryptophycins. *Org. Biomol. Chem.* **2004**, *2*, 1719–1731. [CrossRef]

209. Sinz, C.J.; Rychnovsky, S.D. 4-Acetoxy- and 4-cyano-1,3-dioxanes in synthesis. *Top. Curr. Chem.* **2001**, *216*, 50–93. [CrossRef]

210. Kuznetsov, V.V. Reactions of 1,3-dioxacycloalkanes and their 2-arsena, 2-bora, 2-germa, 2-sila, and 2-thia analogs with nitriles. *Russ. Chem. Bull.* **2005**, *54*, 1543–1551. [CrossRef]

211. Asare-Nkansah, S.; Wünsch, B. Double intramolecular transacetalization of polyhydroxy acetals: Synthesis of conformationally-restricted 1,3-dioxanes with axially-oriented phenyl moiety. *Molecules* **2016**, *21*, 1503. [CrossRef] [PubMed]

212. Kuznetsov, V.V. Computer simulation of conformational transformations of 1,3-dioxanes and their 2-sila and 2-bora analogs. *Russ. J. Org. Chem.* **2014**, *50*, 1227–1246. [CrossRef]

213. Kuznetsov, V.V. Conformational analysis of 1,3-dioxane in nanotubes. *Russ. J. Org. Chem.* **2016**, *52*, 1688–1693. [CrossRef]

214. Raskildina, G.Z.; Spirikhin, L.V.; Zlotskij, S.S.; Kuznetsov, V.V. Conformational analysis of 5-ethyl-5-hydroxymethyl-2,2-dimethyl-1,3-dioxan. *Russ. J. Org. Chem.* **2019**, *55*, 502–507. [CrossRef]

215. Khazhiev, S.Y.; Khusainov, M.A.; Khalikov, R.A.; Kataev, V.A.; Tyumkina, T.V.; Mesheryakova, E.S.; Khalilov, L.M.; Kuznetsov, V.V. Structure and conformational analysis of 5,5-bis(bromomethyl)-2,2-diphenyl-1,3-dioxane. *Russ. J. Org. Chem.* **2020**, *56*, 1–6. [CrossRef]

216. Shainyan, B.A.; Kleinpeter, E. Silacyclohexanes and silaheterocyclohexanes—Why are they so different from other heterocyclohexanes? *Tetrahedron* **2013**, *69*, 5927–5936. [CrossRef]

217. Schultz, G.; Gergö, E.; Kolonits, M.; Hargittai, I. Molecular structure of 2,2-dimethyl-1,3-dioxa-2-silacyclohexane from gas-phase electron diffraction. *J. Mol. Struct.* **1993**, *295*, 143–146. [CrossRef]

218. Bochkor, S.A.; Kuznetsov, V.V. Unusual conformational isomerization of oxygen-containing silacyclohexanes. *Russ. J. Org. Chem.* **2010**, *46*, 945–946. [CrossRef]

219. Bochkor, S.A.; Kuznetsov, V.V. Comparative conformational analysis of 2,2-dimethyl and 2,2,5-trimethyl-1,3-dioxanes and their 2-heteroanalogs with silicon and germanium atoms. *Russ. J. Gen. Chem.* **2016**, *86*, 321–325. [CrossRef]

220. Bochkor, S.A.; Kuznetsov, V.V. 1,3-Dioxa-2-silacyclohexane in nanotubes: Conformational transformations and structural features. *Russ. J. Gen. Chem.* **2016**, *86*, 1300–1305. [CrossRef]

221. Knabe, J.; Büch, H.P.; Biwersi, J. Zyklische Harnstoffe, 1. Mitt.: Racemate und Enantiomere von Hexahydropyrimidin-2-onen: Synthese, Konfiguration und sedativ-hypnotische Wirkung. *Arch. Pharm.* **1993**, *326*, 79–84. [CrossRef] [PubMed]

222. Shutalev, A.D.; Ignatova, L.A. α-Amido(thioamido)alkylation of dithiocarbamic, O-ethyldithiocarbonic, and arylsulfinic acids by 4-hydroxy(alkoxy)hexahydropyrimidine-2-thiones(ones). *Chem. Heterocycl. Compd.* **1991**, *27*, 187–194. [CrossRef]

223. Fesenko, A.A.; Solovyov, P.A.; Shutalev, A.D. A novel convenient synthesis of 5-acyl-1,2-dihydropyrimidin-2-ones via 4-trichloromethyl-1,2,3,4-tetrahydropyrimidin-2-ones. *Tetrahedron* **2010**, *66*, 940–946. [CrossRef]

224. Tamazyan, R.; Ayvazyan, A.; Martirosyan, V.; Avagyan, K.; Martirosyan, A. 1-Benzyl-6-phenylimino-5-(pyrrol-2-ylidene)hexahydropyrimidine-2,4-dione. *Acta Cryst. E* **2008**, *64*, o483. [CrossRef]

225. Kuznetsov, V.V. Conformational behavior of hexahydropyrimidin-2-one and its ammonium and oxonium ions. *Chem. Heterocycl. Compd.* **2011**, *47*, 651–655. [CrossRef]

226. Kuznetsov, V.V. Hexahydropyrimidin-2-one in nanotubes: Structural changes and conformational preferences. *Russ. J. Gen. Chem.* **2017**, *87*, 1461–1465. [CrossRef]

227. Sabirov, D.S.; Garipova, R.R.; Kinzyabaeva, Z.S. Fullerene–1,4-dioxane adducts: A DFT study of the structural features and molecular properties. *Fuller. Nanotub. Carbon Nanostruct.* **2020**, *28*, 154–159. [CrossRef]

228. Yus, M.; González-Gómez, J.C.; Foubelo, F. Diastereoselective allylation of carbonyl compounds and imines: Application to the synthesis of natural products. *Chem. Rev.* **2013**, *113*, 5595–5698. [CrossRef]

229. Partyka, D.V. Transmetalation of unsaturated carbon nucleophiles from boron-containing species to the mid to late d-block metals of relevance to catalytic C–X coupling reactions (X = C, F, N, O, Pb, S, Se, Te). *Chem. Rev.* **2011**, *111*, 1529–1595. [CrossRef] [PubMed]

230. Oestreich, M.; Hartmann, E.; Mewald, M. Activation of the Si–B interelement bond: Mechanism, catalysis, and synthesis. *Chem. Rev.* **2013**, *113*, 402–441. [CrossRef] [PubMed]

231. Brusilovskii, Y.E.; Kuznetsov, V.V. Reactions of cyclic boric acids esters with paraformaldehyde. *Russ. J. Gen. Chem.* **2011**, *81*, 542–544. [CrossRef]

232. Kuznetsov, V.V. Conformational behavior of 1,3,2-dioxaborinane molecule encapsulated in fullerenes. *Russ. J. Gen. Chem.* **2015**, *85*, 198–199. [CrossRef]

233. Reimers, J.R.; McKemmish, L.K.; McKenzie, R.H.; Hush, N.S. Bond angle variations in XH_3 [X = N, P, As, Sb, Bi]: The critical role of Rydberg orbitals exposed using a diabatic state model. *Phys. Chem. Chem. Phys.* **2015**, *17*, 24618–24640. [CrossRef] [PubMed]

234. Li, Y.-Q.; Song, P.; Ma, F.-C. Accurate equilibrium inversion barrier of ammonia by extrapolation to the one-electron basis set limit. *Chin. Phys. B* **2014**, *23*, 023301. [CrossRef]

235. Sharma, R.; Goerigk, L. The INV24 test set: How well do quantum-chemical methods describe inversion and racemization barriers? *Can. J. Chem.* **2016**, *94*, 1133–1143. [CrossRef]

236. Kuznetsov, V.V. Simulation of pyramidal inversion of nitrogen in tetrahydro-1,3-oxazines in polar medium. *J. Struct. Chem.* **2018**, *59*, 1374–1380. [CrossRef]

237. Holleman-Wiberg. *Inorganic Chemistry*; ACADEMIC PRESS: San Diego, CA, USA, 2001; pp. 616–617.

238. Kuznetsov, V.V. Theoretical evaluation of inversion barrier of trimethylamine in nanotubes. *Russ. J. Gen. Chem.* **2013**, *83*, 1453–1454. [CrossRef]

239. Shinsaku, F. Group-theoretical framework for characterizing the ring flipping and *N*-inversion of piperidine derivatives. Extended pseudo-point groups and subsymmetry-itemized enumeration. *Bull. Chem. Soc. Jpn.* **1999**, *72*, 1759–1768. [CrossRef]

240. Anet, F.L.A.; Yavari, I. Nitrogen inversion in piperidine. *J. Am. Chem. Soc.* **1977**, *99*, 2794–2796. [CrossRef]

241. Lambert, J.B.; Featherman, S.I. Conformational analysis of pentamethylene heterocycles. *Chem. Rev.* **1975**, *75*, 611–626. [CrossRef]

242. Carballiera, L.; Pérez-Juste, I. Influence of calculation level and effect of methylation on axial/equatorial equilibria in piperidines. *J. Comput. Chem.* **1998**, *19*, 961–976. [CrossRef]

243. Blackburn, I.D.; Katritzky, A.R.; Takeuchi, Y. Conformation of piperidine and of derivatives with additional ring hetero atoms. *Acc. Chem. Res.* **1975**, *8*, 300–306. [CrossRef]

244. Kuznetsov, V.V. Theoretical estimation of conformational preference of piperidine molecule encapsulated in a nanotube. *Russ. J. Org. Chem.* **2014**, *50*, 143–144. [CrossRef]

245. Rudchenko, V.F.; Shevchenko, V.I.; Kostyanovskii, R.G. 2-Dimethylcarbamoyl-1,3,2-dioxazolidine, 2-dimethylcarbamoyl- and 2*H*-perhydro-1,3,2-dioxazines. *Russ. Chem. Bull.* **1985**, *34*, 1543. [CrossRef]

246. Rudchehko, V.F.; Shevschenko, V.I.; Kostyanovskii, R.G. Geminal systems 33. Reactions of 1,1-dialkoxyureas with electrophiles and nucleophiles. Synthesis of cyclic 1,1-dialkoxyureas and *N,N*-dialkoxyamines. *Russ. Chem. Bull.* **1987**, *36*, 1436–1440. [CrossRef]

247. Kostyanovskii, R.G.; Rudchehko, V.F.; Shtamburg, V.G.; Chervin, I.I.; Nasibov, S.S. Asymmetrical nonbridgehead nitrogen-XXVI[1]: Synthesis, configurational stability, and resolution of *N,N*-dialkoxyamines into antipodes. *Tetrahedron* **1981**, *37*, 4245–4254. [CrossRef]

248. Kuznetsov, V.V. Conformational transformations of of perhydro-1,3,2-dioxazine. *Russ. J. Gen. Chem.* **2012**, *82*, 783–784. [CrossRef]

249. Kuznetsov, V.V. Conformational preference of perhydro-1,3,2-dioxazine inside nanotubes. *Russ. J. Gen. Chem.* **2014**, *84*, 525–530. [CrossRef]

250. Kuznetsova, M.V.; Kuznetsov, V.V. Theoretical estimation of the barrier to pyramidal inversion of ammonia and trimethylamine encapsulated in fullerenes. *Russ. J. Org. Chem.* **2013**, *49*, 1845–1847. [CrossRef]

251. Nitti, A.; Pacini, A.; Pasini, D. Chiral nanotubes. *Nanomaterials* **2017**, *7*, 167. [CrossRef] [PubMed]

252. Liu, J.; Lu, J.; Lin, X.; Tang, Y.; Liu, Y.; Wang, T.; Zhu, H. The electronic properties of chiral carbon nanotubes. *Comput. Mater. Sci.* **2017**, *129*, 290–294. [CrossRef]

253. Wei, X.; Tanaka, T.; Akizuki, N.; Miyauchi, Y.; Matsuda, K.; Ohfuchi, M.; Kataura, H. Single-chirality separation and optical properties of (5,4) single-wall carbon nanotubes. *J. Phys. Chem. C* **2016**, *120*, 10705–10710. [CrossRef]

254. De Faria, C.G.; Grassi, M.; Carvalho, A.C.M. Conformational analysis and electronic structure of chiral carbon and carbon nitride nanotubes. *Mater. Res.* **2011**, *14*, 461–465. [CrossRef]

255. Hemasa, A.L.; Naumovski, N.; Maher, W.A.; Ghanem, A. Application of carbon nanotubes in chiral and achiral separations of pharmaceuticals, biologics and chemicals. *Nanomaterials* **2017**, *7*, 186. [CrossRef]

256. Kameta, N.; Masuda, M.; Shimizu, T. Soft nanotubes acting as confinement effecters and chirality inducers for achiral polythiophenes. *Chem. Commun.* **2016**, *52*, 1346–1349. [CrossRef]

257. Kuznetsov, V.V. Recognition of the *R*- and *S*-isomers of 1-fluoroethanol by a chiral nanotube. *Russ. J. Gen. Chem.* **2015**, *85*, 2813–2815. [CrossRef]

258. Lathan, W.A.; Radon, L.; Hehre, W.J.; Pople, J.A. Molecular orbital theory of the electronic structure of organic compounds. XVIII. Conformations and stabilities of trisubstituted methanes. *J. Am. Chem. Soc.* **1973**, *95*, 699–703. [CrossRef]

259. Kuznetsov, V.V. Recognition of *R*- and *S*-isomers of α-alanine by chiral nanotubes. *Russ. J. Gen. Chem.* **2018**, *88*, 930–934. [CrossRef]

260. Ribeiro da Silva, M.A.V.; Ribeiro da Silva, M.D.M.C.; Santos, A.F.L.O.M.; Roux, M.V.; Foces-Foces, C.; Notario, R.; Guzmán-Mejía, R.; Juaristi, E. Experimental and computational thermochemical study of α-alanine (DL) and β-alanine. *J. Phys. Chem. B* **2010**, *114*, 16471–16480. [CrossRef] [PubMed]

261. Craig, N.C.; Piper, L.G.; Wheeler, V.L. Thermodynamics of cis-trans isomerizations. II. 1-Chloro-2-fluoroethylenes, 1,2-difluorocyclopropanes, and related molecules. *J. Phys. Chem.* **1971**, *75*, 1453–1460. [CrossRef]

262. Cotton, F.A.; Wilkinson, G. *Advanced Inorganic Chemistry*, 4th ed.; John Wiley & Sons Ltd: New York, NY, USA, 1980; p. 434.

263. Jana, J. Relative stabilities of two difluorodiazene isomers: Density functional and molecular orbital studies. *Rep. Theor. Chem.* **2012**, *1*, 1–10. [CrossRef]

264. Banerjee, D.; Ghosh, A.; Chattopadhyay, S.; Ghosh, P.; Chaudhuri, R.K. Revisiting the '*cis*-effect' in 1,2-difluoro derivatives of ethylene and diazene using *ab initio* multireference methods. *J. Mol. Phys.* **2014**, *112*, 3206–3224. [CrossRef]

265. Mourão, Z.S.; Melo, A. Energy decomposition analysis of cis and trans isomers of 1,2-dihaloethylenes and 2-butene. *J. Mol. Struct. Teochem.* **2010**, *946*, 7–12. [CrossRef]

266. Teixeira, F.; Melo, A.; Cordeiro, M.N.D.S. Exploring rare chemical phenomena using fractional nuclear charges: The cis-effect in N_2F_2. *Int. J. Quantum Chem.* **2018**, *118*, e25662. [CrossRef]

267. Kuznetsov, V.V. Theoretical evaluation of relative stability of diazadifluoride isomers in nanotubes. *Russ. J. Gen. Chem.* **2013**, *83*, 140–142. [CrossRef]

268. Kuznetsov, V.V. Theoretical estimation of the stability of *cis*- and *trans*-difluoroethylene in nanotubes. *Russ. J. Org. Chem.* **2013**, *49*, 765–767. [CrossRef]